JCI The Journal of Clinical Investigation

Herpes simplex encephalitis in a patient with a distinctive form of inherited IFNAR1 deficiency

Paul Bastard, … , Jean-Laurent Casanova, Shen-Ying Zhang

J Clin Invest. 2021;131(1):e139980. https://doi.org/10.1172/JCI139980.

Research Article | Immunology | Infectious disease

Graphical abstract

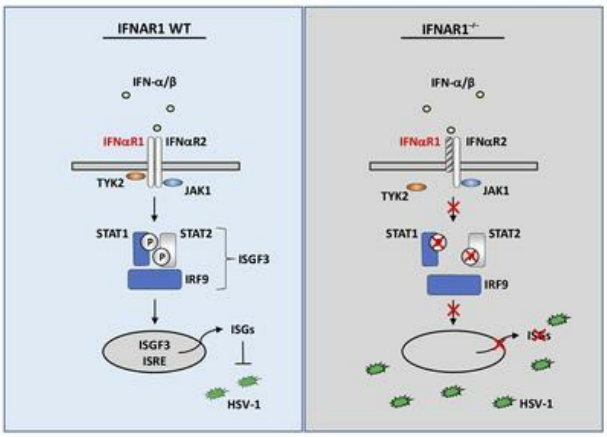

Herpes simplex encephalitis in a patient with a distinctive form of inherited IFNAR1 deficiency

Paul Bastard,[1,2,3] Jeremy Manry,[1,2] Jie Chen,[3] Jérémie Rosain,[1,2] Yoann Seeleuthner,[1,2] Omar AbuZaitun,[4] Lazaro Lorenzo,[1,2] Taushif Khan,[5] Mary Hasek,[3] Nicholas Hernandez,[3] Benedetta Bigio,[3] Peng Zhang,[3] Romain Lévy,[1,2,6] Shai Shrot,[7,8] Eduardo J. Garcia Reino,[3] Yoon-Seung Lee,[3] Soraya Boucherit,[1,2] Mélodie Aubart,[1,9] Rik Gijsbers,[10] Vivien Béziat,[1] Zhi Li,[11] Sandra Pellegrini,[11] Flore Rozenberg,[12] Nico Marr,[5,13] Isabelle Meyts,[14,15,16] Bertrand Boisson,[1,2,3] Aurélie Cobat,[1,2] Jacinta Bustamante,[1,2,3,17] Qian Zhang,[3] Emmanuelle Jouangy,[1,2,3] Laurent Abel,[1,2,3] Raz Somech,[18,19] Jean-Laurent Casanova,[1,2,3,6,20] and Shen-Ying Zhang[1,2,3]

[1]Laboratory of Human Genetics of Infectious Diseases, Necker Branch, INSERM U1163, Paris, France. [2]University of Paris, Imagine Institute, Paris, France. [3]St. Giles Laboratory of Human Genetics of Infectious Diseases, Rockefeller Branch, Rockefeller University, New York, New York, USA. [4]Ambulatory Pediatrics, Nablus, Palestinian. [5]Research Branch, Sidra Medicine, Doha, Qatar. [6]Pediatric Immunology-Hematology Unit, Assistance Publique–Hôpitaux de Paris (AP-HP), Necker Hospital for Sick Children, Paris, France. [7]Department of Diagnostic Imaging, Sheba Medical Center, Ramat Gan, Israel. [8]Sackler School of Medicine, Tel Aviv University, Tel Aviv, Israel. [9]Department of Pediatric Neurology, Necker Hospital for Sick Children, University of Paris, Paris, France. [10]Laboratory of Viral Vector Technology and Gene Therapy and Leuven Viral Vector Core, Faculty of Medicine, KU Leuven, Leuven, Belgium. [11]Unit of Cytokine Signaling, Pasteur Institute, INSERM U1221, Paris, France. [12]Laboratory of Virology, University of Paris, AP-HP, Cochin Hospital, Paris, France. [13]College of Health and Life Sciences, Hamad Bin Khalifa University, Doha, Qatar. [14]Laboratory of Inborn Errors of Immunity, Department of Immunology, Microbiology and Transplantation, KU Leuven, Leuven, Belgium. [15]Department of Pediatrics, Jeffrey Modell Diagnostic and Research Network Center, University Hospitals Leuven, Leuven, Belgium. [16]Precision Immunology Institute and Mindich Child Health and Development Institute at the Icahn School of Medicine at Mount Sinai, New York, New York, USA. [17]Center for the Study of Primary Immunodeficiencies, Necker Hospital for Sick Children, AP-HP, Paris, France. [18]Pediatric Department and Immunology Unit, Edmond and Lily Safra Children's Hospital, Jeffrey Modell Foundation Center, Sheba Medical Center, Tel HaShomer, Israel. [19]Sackler School of Medicine, Tel Aviv University, Tel Aviv, Israel. [20]Howard Hughes Medical Institute, New York, New York, USA.

Inborn errors of TLR3-dependent IFN-α/β– and IFN-λ–mediated immunity in the CNS can underlie herpes simplex virus 1 (HSV-1) encephalitis (HSE). The respective contributions of IFN-α/β and IFN-λ are unknown. We report a child homozygous for a genomic deletion of the entire coding sequence and part of the 3′-UTR of the last exon of *IFNAR1*, who died of HSE at the age of 2 years. An older cousin died following vaccination against measles, mumps, and rubella at 12 months of age, and another 17-year-old cousin homozygous for the same variant has had other, less severe, viral illnesses. The encoded IFNAR1 protein is expressed on the cell surface but is truncated and cannot interact with the tyrosine kinase TYK2. The patient's fibroblasts and EBV-B cells did not respond to IFN-α2b or IFN-β, in terms of STAT1, STAT2, and STAT3 phosphorylation or the genome-wide induction of IFN-stimulated genes. The patient's fibroblasts were susceptible to viruses, including HSV-1, even in the presence of exogenous IFN-α2b or IFN-β. HSE is therefore a consequence of inherited complete IFNAR1 deficiency. This viral disease occurred in natural conditions, unlike those previously reported in other patients with IFNAR1 or IFNAR2 deficiency. This experiment of nature indicates that IFN-α/β are essential for anti–HSV-1 immunity in the CNS.

Introduction

Herpes simplex virus 1 (HSV-1) is an α-herpesvirus that infects about 75% of the general population by the age of 18 years (1, 2). Following primary infection, it typically establishes latency in trigeminal ganglia, whence it may occasionally reactivate, typically manifesting as labial mucocutaneous lesions. In about 1–2 per 10,000 infected individuals, HSV-1 can reach the brain via the olfactory bulb or trigeminal nerve, causing life-threatening herpes simplex encephalitis (HSE) of the forebrain or brainstem, respectively (3). HSE is the most common sporadic viral encephalitis affecting otherwise healthy humans, at least in Western countries. Its incidence peaks between the ages of 3 months and 6 years, earlier than would be predicted from age at primary infection alone (1). During HSE, the infection is restricted to the CNS, with the forebrain affected in about 95% of cases and the brainstem affected in the remaining approximately 5% of cases (1, 4). There are usually no mucocutaneous lesions, no detectable viremia, and no lesions of internal organs other than the brain. The advent of acyclovir treatment has decreased the mortality of HSE from about 75% to about 20% (5). However, 40%–60% of survivors suffer mild-to-severe (10%–20%) neurological sequelae (6–8). With the exception of the identification of the causal virus, the pathogenesis of HSE remained unexplained until 2006–2007,

Authorship note: JM, JC, JR, and YS contributed equally to this work. JLC and SYZ contributed equally to this work.
Conflict of interest: The authors have declared that no conflict of interest exists.

Submitted: May 6, 2020; **Accepted:** September 17, 2020; **Published:** January 4, 2021.
Reference information: *J Clin Invest*. 2021;131(1):e139980.
https://doi.org/10.1172/JCI139980.

when inborn errors of UNC-93B–dependent TLR3 immunity were found to underlie the development of isolated forebrain HSE in some children (9, 10). Other autosomal recessive (AR) or autosomal dominant (AD) inborn errors have since been reported to underlie forebrain HSE through an impairment of the TLR3-responsive pathway (9, 11–15) or snoRNA31 function (16). Moreover, an AR partial DBR1 deficiency has been shown to impair RNA lariat metabolism and to underlie brainstem viral encephalitis, including brainstem HSE (17).

Germline mutations of *UNC93B1*, *TLR3*, *TRIF*, *TRAF3*, *TBK1*, *IRF3*, and other TLR3 pathway genes have been identified in children with isolated forebrain HSE (10–13, 18–21). These mutations impair the TLR3-dependent induction of both IFN-α/β and IFN-λ in responses to dsRNA in dermal fibroblasts and induced pluripotent stem cell–derived (iPSC-derived) cortical neurons and oligodendrocytes, associated with enhanced susceptibility to HSV-1 infection (15). By contrast, iPSC-derived trigeminal neurons are naturally permissive to HSV-1 infection, regardless of their TLR3 genotype (14). Most blood leukocyte subsets respond to dsRNA and HSV-1 in a TLR3-independent manner (11). In patients with TLR3 pathway mutations, penetrance for HSE is incomplete, even in individuals seropositive for HSV-1 (22). Moreover, patients with TLR3 deficiency are also prone to influenza A virus–associated acute respiratory distress syndrome, with incomplete penetrance, possibly due to impairment of the TLR3-dependent induction of IFN-α/β and -λ in pulmonary epithelial cells (23). Finally, a child with an X-linked hemizygous *NEMO* mutation impairing IFN-α/β, -γ, and -λ production, and another child with AR complete STAT1 deficiency impairing cellular responses to IFN-α/β, -γ, and -λ, both developed HSE and mycobacterial disease (21, 24). Impaired IFN-γ immunity accounted for their mycobacterial disease, as all genetic etiologies of Mendelian susceptibility to mycobacterial disease disrupt the production of or the response to IFN-γ (25, 26). Together, these findings suggest that TLR3-dependent, IFN-α/β– and/or IFN-λ–mediated immunity is crucial for the control of HSV-1 infection in the forebrain (27, 28). However, the respective contributions of IFN-α/β and -λ remain unclear. We thus studied other patients with HSE by whole-exome sequencing, searching for mutations of the genes encoding the receptors for these 2 types of antiviral IFN.

Results

A fatal case of HSE in a patient from a large consanguineous family. We studied a girl (P1, IV.2), born to first-cousin parents of Arab ancestry living in Palestinian territory (Figure 1A and Supplemental Methods; supplemental material available online with this article; https://doi.org/10.1172/JCI139980DS1). She was healthy and developed normally until the age of 13 months, when she developed a prolonged fever, for which she was hospitalized, received intravenous immunoglobulins, and recovered. At the age of 16 months, she was hospitalized again for gingivostomatitis and aseptic meningitis (herpes simplex virus PCR was not performed). At the age of 19 months, she was readmitted for fever, oral lesions, and focal seizures. HSV-1 PCR was positive on cerebrospinal fluid (CSF), a brain electroencephalogram showed signs of epilepsy in the left temporal lobe, and brain MRI displayed lesions in the left parietal lobe and left temporal-occipital lobe (Figure 1B and Supplemental Figure 1A). The patient was diagnosed with HSE and treated with intravenous acyclovir. Despite this treatment, HSV-1 PCR on CSF remained positive, and the patient remained in a semiconscious state. She died 1 month later, due to severe neurological sequelae. A cousin of P1 (P2, IV.12, also born to first-cousin parents) had suffered from 2 episodes of aseptic meningitis at the ages of 6 and 10 months, with negative cultures. HSV-1 was suspected but not proven to be causal, and the patient recovered following acyclovir treatment. He developed parotitis at the age of 14 years, followed by bilateral hearing loss requiring cochlear implants. Mumps virus infection was strongly suspected to be responsible for this episode, as suggested retrospectively by the high levels of anti–mumps virus IgG in the patient's blood at a follow-up visit at the age of 17 years (Supplemental Figure 1B). The patient was 17 years old at time of writing and had developed no other severe infections. Another cousin of P1 (P3, a sibling of P2) died at the age of 12 months following a severe adverse reaction to measles, mumps, and rubella (MMR) vaccination (Figure 1A). P1 had developed a fever following MMR vaccination at the age of 12 months, but it resolved spontaneously. The other children of this large kindred, including P2, were not vaccinated against MMR, in accordance with the wishes of the parents, following the death of P3 after MMR vaccination.

A homozygous large deletion from intron 10 to exon 11 of IFNAR1 in P1 and P2. We performed whole-exome sequencing (WES) on leukocyte genomic DNA (gDNA) from the index case (P1). WES revealed a high rate of homozygosity (5.9%) in the patient, consistent with her parents being first cousins. We therefore hypothesized that P1 may have developed HSE due to an AR disorder. We tested this hypothesis by searching for homozygous single-nucleotide variants (SNVs). We filtered out common variants (minor allele frequency >0.01), variants predicted to be benign (combined annotation-dependent depletion [CADD] score below the mutation significance cutoff) within the 95% confidence interval (29), and variants occurring in highly damaged genes (those with a gene damage index >13.84; ref. 30) (Supplemental Figure 1D). P1 carried nonsynonymous homozygous SNVs in 6 genes meeting the filtering criteria (Supplemental Figure 1E). None of these genes had previously been associated with immunity or had a CNS-specific pattern of expression. We then analyzed copy number variants with HMZDelFinder software (31). We found a 1675-bp homozygous deletion, Chr2 1(GRCh37):g.34,726,420_34,728,094del, removing the region flanking intron 10 and part of exon 11 of *IFNAR1* (Supplemental Figure 1F). The deletion was confirmed by Sanger sequencing of gDNA from the whole blood and dermal fibroblasts of the patient (Figure 1, C and D). The cousin who suffered from 2 episodes of suspected HSV meningitis (P2) was also homozygous for the large deletion. The parents of P1 and P2 each carried the deletion in the heterozygous state, and all other family members tested were either heterozygous for the deletion or homozygous WT (Figure 1, A and C). The sibling of P2 who died following a severe adverse reaction to MMR vaccination (P3) was not tested, as no gDNA was available. This *IFNAR1* variant was not found in any public databases (1000 Genomes, dbSNP, Database

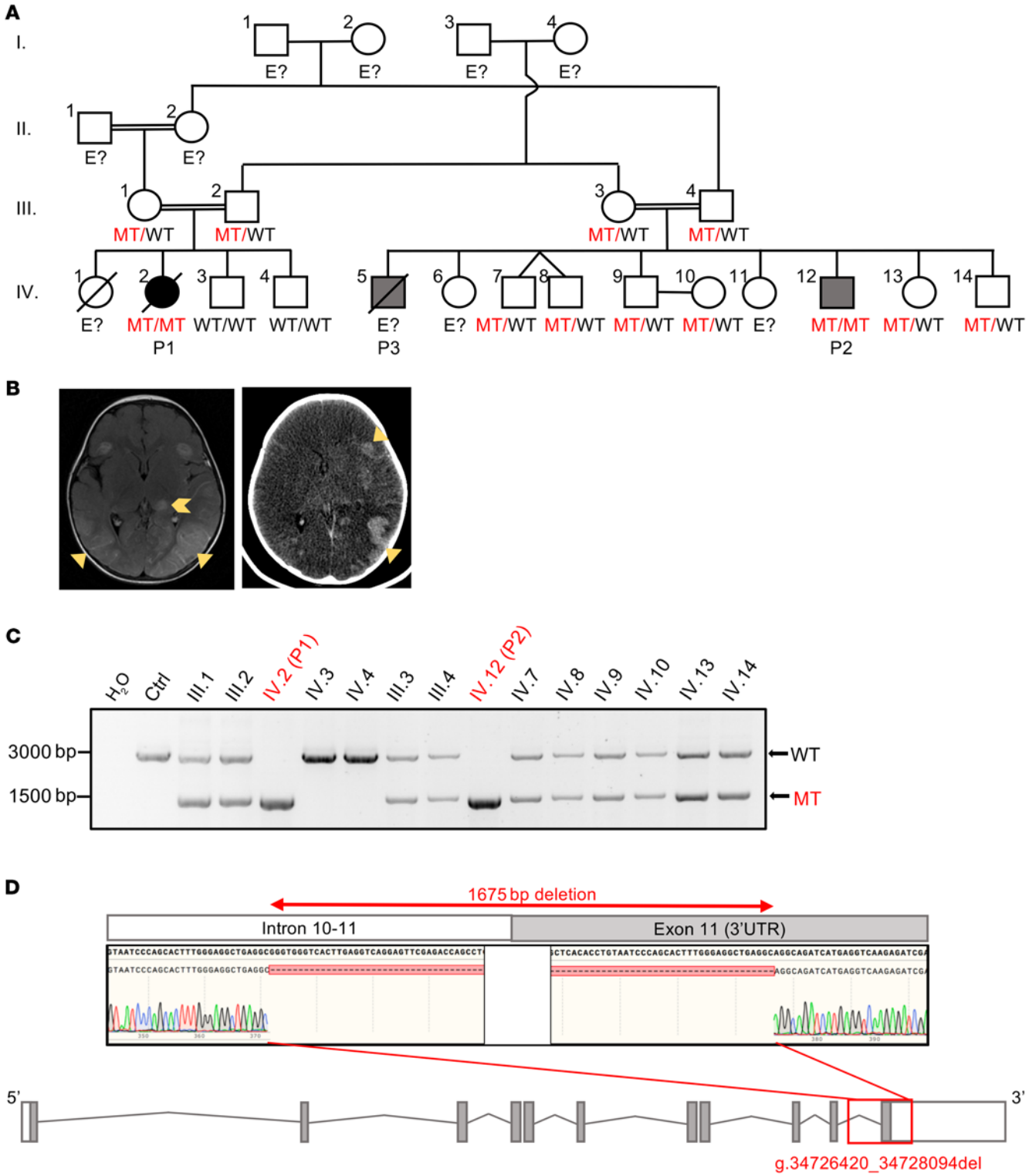

Figure 1. Homozygous deletion in *IFNAR1* in a patient who died from HSE and her cousin. (**A**) Family pedigree showing the segregation of the *IFNAR1* mutant (MT) allele. Double lines connect the 2 parents with consanguinity. The filled black symbol indicates the proband (patient 1, P1) with HSE, the filled gray symbols indicate individuals with viral diseases other than HSE, and the open symbols indicate healthy family members. E?, unknown *IFNAR1* genotype. (**B**) Brain imaging showing HSE lesions in P1. Left: Post-contrast T2-FLAIR image showing diffuse cortical and subcortical edema on temporo-occipital regions accompanied by leptomeningeal enhancement (yellow triangles), compatible with meningoencephalitis. There are also parenchymal lesions, involving the left thalamus and base of the frontal lobes, indicated by yellow arrowhead. Right: Noncontrast head CT, performed 7 days later, showing diffuse brain edema with multiple parenchymal hemorrhages in the edematous areas previously identified (yellow triangles). (**C**) *IFNAR1* from leukocyte gDNA from the patients and other relatives, amplified by PCR with a forward primer binding to exon 10 and a reverse primer binding to the 3′-UTR part of exon 11. The result shown is representative of 2 independent experiments. (**D**) Top: Sanger sequencing results for *IFNAR1* from patient leukocyte gDNA. Bottom: Schematic diagram of the *IFNAR1* gene in the gDNA, with 11 coding exons, and a red box representing the location of the deletion found in the patients. The result shown is representative of 3 independent experiments on 2 independently drawn samples.

of Genomic Variants, and gnomAD SVs v2; refs. 32–37) or in our in-house database of 7151 exomes. P1 and her cousin (P2) are therefore homozygous for a private large deletion extending from intron 10 to exon 11 (the last coding exon) of *IFNAR1*.

The deletion in IFNAR1 is predicted to be pathogenic. *IFNAR1* encodes one of the 2 chains of the receptor of type I IFNs (38–40). The IFNAR1/IFNAR2 receptor complex is the sole sensor for all 17 subtypes of human type I IFNs, including 13 IFN-α, 1 IFN-β, 1 IFN-ε, 1 IFN-κ, and 1 IFN-ω (41). No *IFNAR1* variants predicted to be loss of function are recorded in the homozygous state in any public databases. We recently reported AR complete IFNAR1 deficiency in 2 unrelated kindreds with severe adverse reactions to live attenuated measles or yellow fever vaccine (42). IFNAR1 deficiency has not been associated with any severe viral infection occurring in natural conditions. The 1675-bp deletion in *IFNAR1* found in P1 and P2 removes 1202 bp of the region flanking intron 10, and part of exon 11, including the entire 234-bp coding sequence of this exon and 239 bp of the 3′-UTR (Figure 1D). The breakpoints of the patient's deletion were located in 2 different Alu elements: an *Alu*Sz element in intron 10 and an *Alu*Sc element in the 3′-UTR part of exon 11, which displayed a junctional microhomology of 32 bp (Supplemental Figure 2A), suggesting that this deletion arose from an *Alu-Alu*–mediated event. This deletion comprises all of the coding sequence of exon 11 (residues g.34,727,622 to g.34,727,852), and the corresponding allele would probably encode a mutant (MT) protein lacking most of the intracellular domain (77 of 100 amino acids), including box 2, the major TYK2-interacting domain of IFNAR1 (at residues Leu490–Asn507) (43). Given the critical role of IFNAR1 in ligand binding, and the high likelihood of large homozygous deletions impairing receptor function, we hypothesized that the homozygous *IFNAR1* deletion underlies both AR IFNAR1 deficiency and the pathogenesis of HSE in P1, and that of other viral illness documented or suspected in P1 and P2.

The IFNAR1 deletion detected in gDNA leads to aberrant splicing of the IFNAR1 mRNA. The *IFNAR1* deletion detected in P1 encompassed most of intron 10 and all of the coding sequence of exon 11, together with part of the 3′-UTR sequence. We therefore hypothesized that it would lead to aberrant splicing. In silico splicing-site prediction models were not informative, probably owing to the large size of the deletion. Using mRNA extracted from peripheral blood mononuclear cells (PBMCs) from a healthy control and P2, who is also homozygous for the deletion, we amplified the C-terminal part of the *IFNAR1* cDNA containing exon 10, the coding part of exon 11, and 986 bp from the 3′-UTR (Supplemental Figure 2B). Sanger sequencing of the PCR products following TOPO-TA cloning showed that, unlike cDNA from the healthy control, which contained 100% WT sequence, 100% of the reads from the cDNA obtained from P2 lacked the 234 bp of the coding region of exon 11 and 239 bp of the 3′-UTR, but displayed a 97-bp insertion in intron 10 (c.1440+331_*239del.1440+234_+330ins) (Figure 2, A and B). This 97-bp insertion (g.34,726,323_ 34,726,419) corresponds to the sequences located directly 5′ to the start of the deletion (g.34,726,420_34,728,094del), suggesting that a new splicing site (AG, g.34,726,321-g.34,726,322) is created (Supplemental Figure 2C). We performed total RNA-Seq on PBMCs and primary dermal fibroblasts from healthy controls and P2 to exclude the possibility that other less frequent transcripts were produced but had remained undetected. The results obtained were consistent with our initial findings (Figure 2C). Therefore, in both blood cells and dermal fibroblasts, this deletion in *IFNAR1* led to complete aberrant splicing of the *IFNAR1* mRNA, which, if translated, would generate a protein with a C-terminal truncation (p.Y481_insIHCGICFPV*) lacking the residues (aa 490–507) known to be crucial for IFNAR1 interaction with TYK2 (43) (Figure 2D).

The MT IFNAR1 protein is expressed at the cell surface, truncated, and does not bind TYK2. IFNAR1 is ubiquitously expressed throughout the human body, on both hematopoietic and nonhematopoietic cells (44, 45). It is a cell membrane protein that constitutively binds TYK2 via its C-terminal cytoplasmic tail, whereas IFNAR2 constitutively binds JAK1 (40, 46–48). We first studied the expression of the MT IFNAR1 by plasmid-mediated overexpression in HEK293T cells. Following the transient transfection of cells with plasmids containing the WT or MT *IFNAR1* cDNA, similar levels of *IFNAR1* mRNA were detected for the WT and MT IFNAR1 by real-time quantitative PCR (qPCR) with probes covering exons 3–4 or 6–7 of *IFNAR1*, whereas no *IFNAR1* cDNA was detected for the MT *IFNAR1* when a probe covering exons 10–11 of *IFNAR1* was used, consistent with the deletion in exon 11 (Figure 3A). Western blot analysis of these cell extracts with an antibody specific for the N-terminal region of IFNAR1 revealed 2 smeary bands for the WT and MT IFNAR1 (Figure 3B). Following PNGase F treatment, bands with a lower MW were detected, suggesting that the larger bands corresponded to glycosylated forms of IFNAR1. The MT IFNAR1 protein had a lower MW but was as abundant as WT IFNAR1. However, only the WT IFNAR1 protein was detected with an antibody against the C-terminus of IFNAR1, confirming that the MT IFNAR1 was produced as a C-terminally truncated protein (Figure 3C). We then analyzed the cell surface expression of the WT and MT IFNAR1 by FACS (in HEK293T cells) and confocal microscopy (in HeLa cells). In these overexpression systems, the MT IFNAR1 was expressed normally at the cell plasma membrane (Figure 3, D–F). As a control, the previously reported p.V225AfsX228 IFNAR1 mutant (referred to here as p.V225fs) (42) was included in these overexpression experiments, and was shown to be truncated, and not expressed at the cell membrane (Figure 3, B–F). Finally, we tested the hypothesis that the MT IFNAR1 of the patients could not interact with TYK2, owing to the absence of the TYK2 interaction domain. By coimmunoprecipitation of TYK2 and IFNAR1 in HEK293T cells overexpressing both these proteins, we showed that the WT IFNAR1 could interact with TYK2, whereas neither the MT IFNAR1 from these patients nor the previously reported p.V225fs mutant displayed such an interaction (Figure 3G and Supplemental Figure 3, A and B). In summary, overexpression of the mutant cDNA in vitro suggested that the patients' MT IFNAR1 was expressed at the cell membrane as a truncated protein unable to interact with TYK2.

The patient cells express a truncated IFNAR1 and do not respond to IFN-α/β. The binding of IFN-α/β to the receptor complex leads to the activation of TYK2 and JAK1, leading in turn to the phosphorylation of STAT1 and STAT2, which form the trimeric ISGF3 complex with IRF9, as well as the phosphorylation of STAT3,

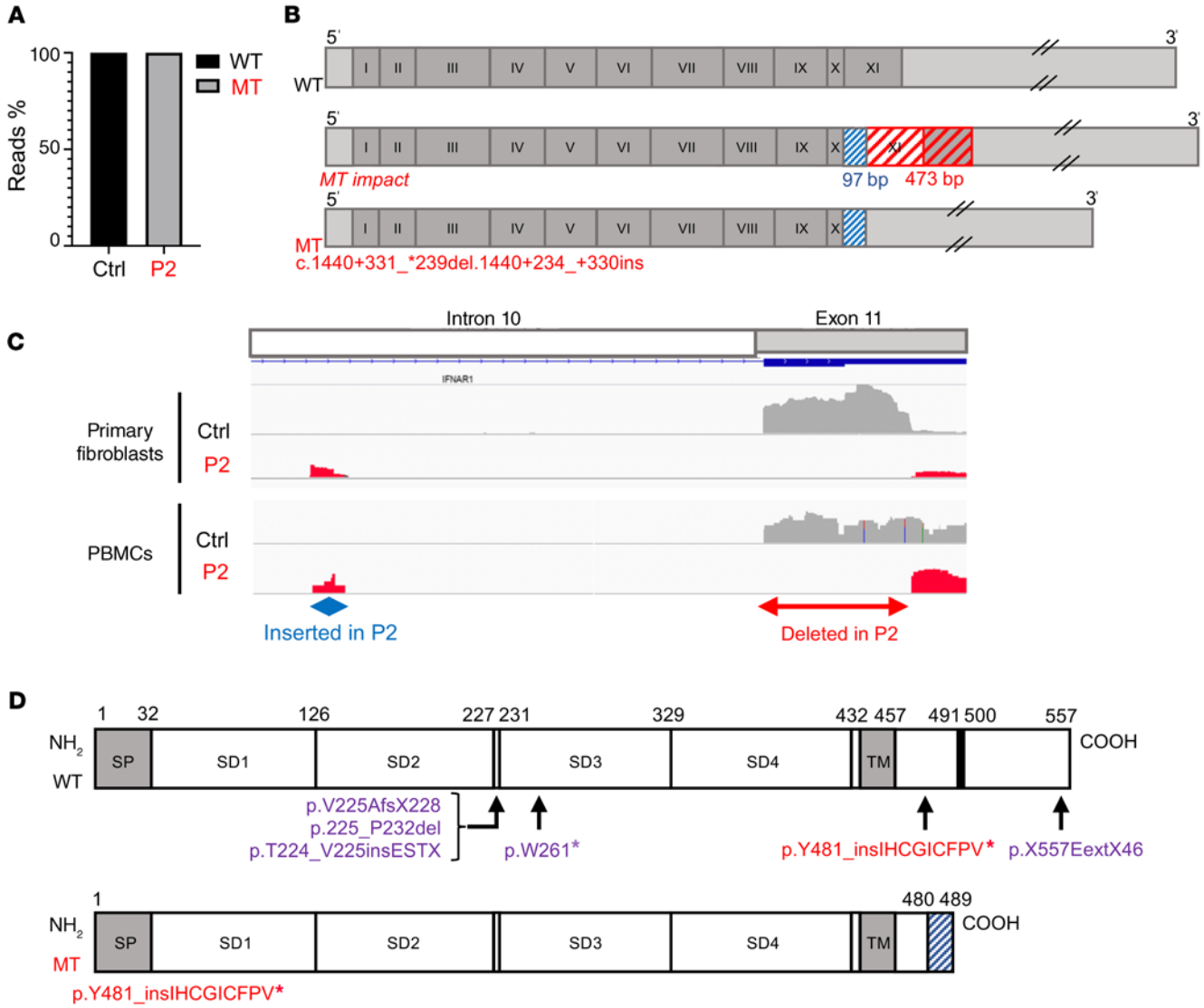

Figure 2. The *IFNAR1* deletion leads to aberrant cDNA splicing. (**A**) cDNA TOPO cloning and sequencing results demonstrating complete aberrant splicing of *IFNAR1* in PBMCs from P2. At least 100 transcripts were sequenced for the patient and the control. The result shown is the sum of 2 independent experiments. (**B**) Schematic diagram of the full-length cDNA of WT and MT *IFNAR1*. Sequencing results demonstrated aberrant splicing and an absence of the coding sequence of *IFNAR1* exon 11 in PBMCs from P2. The blue box indicates the 97-bp intronic insertion. The red box indicates the 473-bp deletion. The exons are numbered in roman numerals (I–XI). The 5′- or 3′-UTR is shown in light gray, and the coding sequences of the exons are shown in dark gray. (**C**) RNA-Seq results for primary fibroblasts (top) or PBMCs (bottom) showing the coverage of *IFNAR1* from intron 10 to exon 11, in healthy controls and P2, demonstrating an insertion and the deletion of the coding sequence of exon 11 and part of the 3′-UTR. For primary fibroblasts, the results shown are representative of 5 technical replicates (corresponding to different RNA-Seq conditions). (**D**) Schematic diagram of the WT and MT IFNAR1 proteins, with the 4 fibronectin type III subdomains (SD1–SD4) and the TYK2 interaction domain (in black). The signal peptide is denoted "SP" and the transmembrane domain "TM." The mutation reported in this study is indicated in red, and previously reported mutations are indicated in violet.

which forms homodimers. This complex migrates to the nucleus, where it promotes the expression of IFN-stimulated genes (ISGs) (40, 49–51). We therefore analyzed the expression of IFNAR1 in fibroblasts from P2, and cellular responses to stimulation with IFN-α2b or IFN-β. SV40-transformed fibroblasts (SV40-fibroblasts) from P2 had low levels of *IFNAR1* mRNA, about half those in the cells of healthy controls (Figure 4A), suggesting nonsense-mediated mRNA decay (52). Consistent with the deletion in exon 11 of the *IFNAR1* gene, no *IFNAR1* mRNA was detected by real-time qPCR when a probe covering exons 10–11 was used (Figure 4A). Consistent with the low levels of *IFNAR1* mRNA in P2's fibroblasts, Western blotting for IFNAR1 in these cells revealed the presence of smaller amounts of a protein with a lower MW than that in healthy control cells (Figure 4B). Moreover, flow cytometry showed that IFNAR1 was expressed on the cell surface of SV40-fibroblasts from P2, albeit at slightly lower levels than in controls (Figure 4C). SV40-fibroblasts from a previously reported IFNAR1-deficient patient (homozygous for p.V225fs) were used as a negative control. The level of IFNAR2 expression was normal in the cells of the patient homozygous for the MT IFNAR1 (Supplemental Figure 4A). We then studied the responses of the patient cells to IFN-α/β

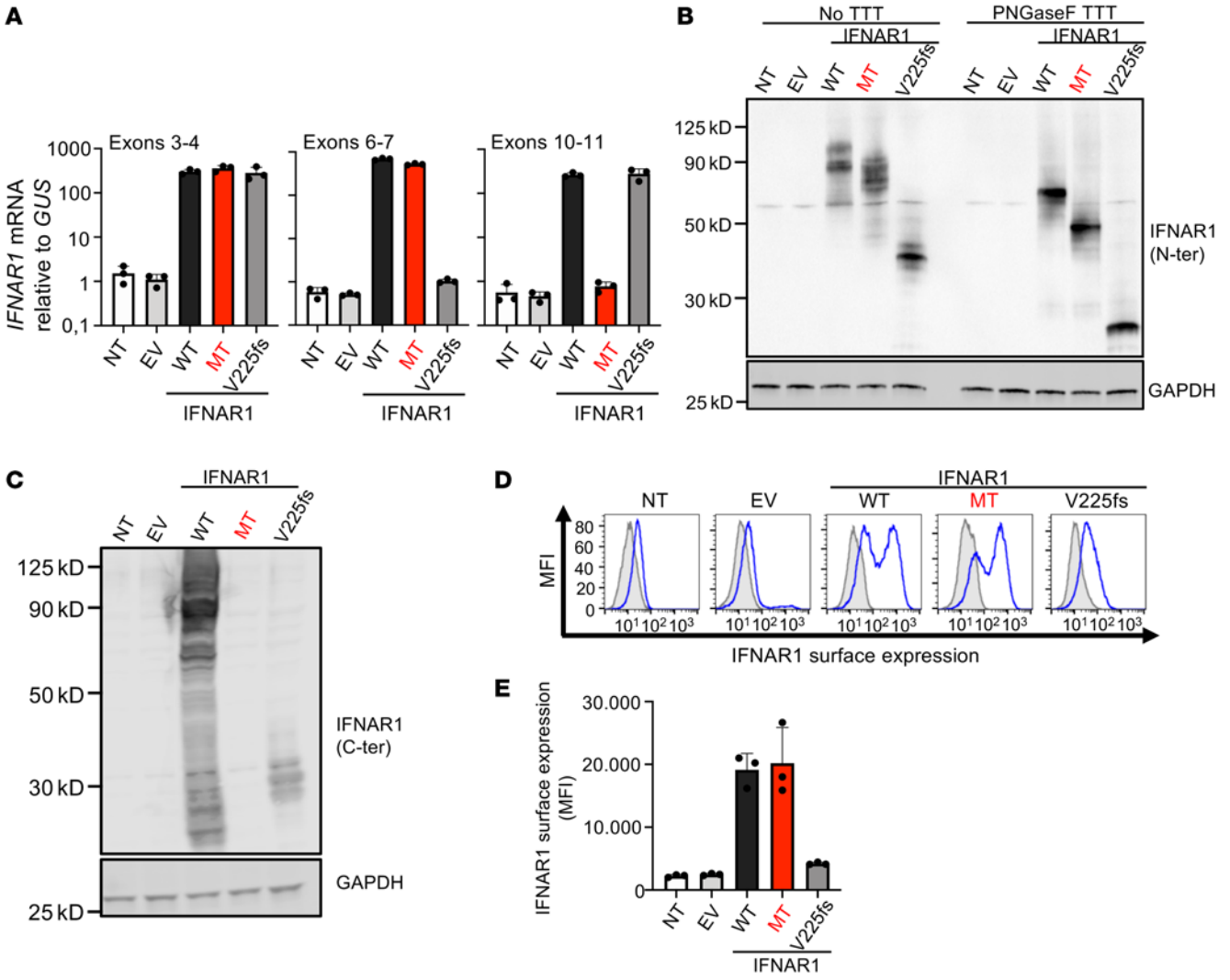
A
IFNAR1 mRNA relative to GUS
Exons 3-4
Exons 6-7
Exons 10-11
1000
100
10
1
0,1
NT
EV
WT
MT
V225fs
IFNAR1
B
No TTT
PNGaseF TTT
IFNAR1
125 kD
90 kD
50 kD
30 kD
25 kD
IFNAR1 (N-ter)
GAPDH
C
IFNAR1 (C-ter)
GAPDH
D
MFI
IFNAR1 surface expression
E
IFNAR1 surface expression (MFI)
30.000
20.000
10.000
0
F
IFNAR1
WGA
Merged
10um
G
Pulldown with IFNAR1 Ab
EV
TYK2
IFNAR1 WT
IFNAR1 MT
IFNAR1 V225fs
TYK2
IFNAR1

Figure 3. The MT IFNAR1 protein is expressed on the cell surface, truncated, and does not bind TYK2. (**A**) Real-time qPCR for *IFNAR1* in HEK293T cells transiently transfected with *IFNAR1* cDNA constructs; *GUS* was used as an expression control. Mean value and SD from 3 independent experiments with technical duplicates in each experiment. (**B**) Western blot (WB) of IFNAR1 in HEK293T cells transiently transfected with *IFNAR1* cDNA constructs, and the same samples treated with PNGase F to inhibit glycosylation. An antibody recognizing the N-terminal (N-ter) part of the IFNAR1 protein was used. GAPDH was used as a loading control. A representative blot from 3 independent experiments is shown. NT, nontransfected; EV, empty vector; V225fs, variant of the previously reported IFNAR1$^{-/-}$ patient. TTT, treatment. (**C**) WB of IFNAR1 in HEK293T cells transiently transfected with *IFNAR1* constructs. An antibody recognizing the C-terminal (C-ter) part of the protein was used. GAPDH was used as a loading control. A representative blot from 2 independent experiments is shown. (**D**) Extracellular FACS staining and mean fluorescence intensity (MFI) of IFNAR1 in HEK cells transiently transfected with *IFNAR1* cDNA constructs, with an antibody recognizing the N-terminus of the protein. Cells were not permeabilized. Results representative of 3 independent experiments are shown. (**E**) MFI of IFNAR1 surface expression, represented graphically. Mean values and SD from 3 independent experiments are shown. (**F**) Immunofluorescence staining, as assessed by confocal microscopy in HeLa cells transiently transfected with *IFNAR1* cDNA constructs. An antibody against the N-terminus of IFNAR1 was used (green), and membranes were stained for wheat germ agglutinin (WGA) (purple). The nuclei were stained with DAPI (blue). The images shown are representative of 3 independent experiments. (**G**) WB for TYK2 and IFNAR1 after coimmunoprecipitation from protein extracts of HEK293T cells cotransfected with WT or MT *IFNAR1* cDNA constructs and WT TYK2. The images presented are representative of 3 independent experiments.

stimulation, in primary fibroblasts and SV40-fibroblasts. Consistent with the lack of interaction with TYK2, the stimulation of patient SV40-fibroblasts with IFN-α2b or IFN-β for 15 minutes did not induce the phosphorylation of STAT1, STAT2, or STAT3 in patient cells, as already reported in another IFNAR1-deficient patient (Figure 4, D and E, and Supplemental Figure 4, B–D). Similar results were obtained for primary fibroblasts (Supplemental Figure 4, E–G). Moreover, the late response to IFN-α/β was also impaired in patient SV40-fibroblasts, as shown by the lack of HLA class I induction 48 hours after stimulation with IFN-α2b or IFN-β (Figure 4F and Supplemental Figure 4H). By contrast, the response to IFN-γ was normal in IFNAR1-deficient fibroblasts but abolished in IFNGR1-deficient cells from a previously reported patient (53) (Figure 4, D–F; and Supplemental Figure 4, B–H). The IFN-α/β–induced phosphorylated STAT1 (p-STAT1) phenotype in the SV40-fibroblasts of P2 was rescued by overexpression of the WT IFNAR1 but not by overexpression of the MT or p.V225fs IFNAR1 (Supplemental Figure 4I). Finally, similar results were obtained for mRNA levels in the PBMCs of P2, mRNA levels in EBV-B cells, cell surface and total protein IFNAR1 protein levels (Figure 5, A–D), and the IFN-α/β–induced p-STAT1, p-STAT2, and p-STAT3 phenotypes of EBV-B cells (Figure 5E and Supplemental Figure 5, A–C). As a control, responses to IFN-γ and IFN-λ were normal in the EBV-B cells of the patient (Figure 5E and Supplemental Figure 5, A–C). In all these experiments, IFNAR2-, IFNGR1-, STAT1-, or STAT2-deficient fibroblasts or EBV-B cells from previously reported patients (53–55) were included as negative controls for the lack of IFNAR2, IFNGR1, STAT1, or STAT2 expression and/or activation, respectively (Figure 4, C–F; Figure 5, C–E; Supplemental Figure 4, A–H; and Supplemental Figure 5, A–C). The results obtained suggested that the homozygous deletion in *IFNAR1* present in P1 and P2 led to AR complete IFNAR1 deficiency, at least for phosphorylation of the known molecules directly mediating activation of the downstream pathway of IFNAR1, in fibroblasts and EBV-B cells.

No induction of ISGs in response to IFN-α/β in patient fibroblasts and EBV-B cells. For confirmation of the defective responses to IFN-α/β in patient cells, we first performed real-time qPCR to assess the induction of *MX1* and *IFIT1* in control and patient SV40-fibroblasts and EBV-B cells in response to stimulation with IFN-α2b or -β. We found that this response was abolished in both SV40-fibroblasts and EBV-B cells from P2, after 2 hours and 8 hours of stimulation, whereas the response to IFN-γ was conserved in these cells and abolished in cells from a patient with AR complete IFNGR1 deficiency (53) (Figure 6, A and B). As a control, the induction of *MX1* and *IFIT1* was also impaired following stimulation with IFN-α2b, IFN-β, or IFN-γ, in cells from a patient with AR complete STAT1 deficiency (54) (Figure 6, A and B). These results confirmed that the homozygous deletion in *IFNAR1* resulted in impaired responses to IFN-α2b and IFN-β, including ISG induction, in fibroblasts and EBV-B cells. However, it remained unclear whether cells homozygous for the plasma membrane–expressed truncated MT IFNAR1 retained some response to IFN-α/β that could lead to induction of other ISGs that we did not measure by real-time qPCR, via the direct induction of responses not dependent on p-STAT (56, 57), or through indirect responses via interaction with IFNAR2 at the cell membrane. It is also unknown whether there is a residual IFN-α/β response mediated by functional IFNAR2 alone, in the absence of functional IFNAR1. We addressed these questions at the genome-wide (GW) level, by performing a transcriptomic analysis based on total RNA-Seq in patient and control primary fibroblasts after stimulation for 2 hours and 8 hours with IFN-α2b. The fibroblasts of the patients studied here, like those of the previously reported IFNAR1 p.V225fs patient, displayed a complete absence of GW transcriptomic response to IFN-α2b at both time points (Figure 6, C and D; and Supplemental Figure 6, A and B). As a control, 2 hours or 8 hours of IFN-γ stimulation induced normal transcriptomic responses in these IFNAR1-deficient fibroblasts, whereas no such responses were observed in the cells of a patient with AR complete IFNGR1 deficiency (Figure 6, C and D; and Supplemental Figure 6, A and B) (53). These results confirm that the intracellular domain of IFNAR1 is required for signaling in all responses to IFN-α/β in human fibroblasts. Finally, the overexpression of exogenous WT, but not MT, IFNAR1 in patient SV40-fibroblasts rescued the induction of the various ISGs tested (*IFIT1* and *MX1*) upon IFN-α2b or IFN-β stimulation (Supplemental Figure 6C). Together, these results confirmed that the homozygous deletion in *IFNAR1* abolished responses to both IFN-α2b and IFN-β in fibroblasts and EBV-B cells.

Enhanced susceptibility of patient fibroblasts to viruses in the presence or absence of IFN-α/β. In our previous studies, we used human dermal fibroblasts as a surrogate cell type for assessing non–hematopoietic cell–intrinsic immunity to viruses, including HSV-1, mediated by TLR3, IFN, or other mechanisms (10, 11, 13, 19, 20). TLR3-, STAT1-, or IFNAR1-deficient patient SV40-fibroblasts have been shown to display enhanced susceptibility to

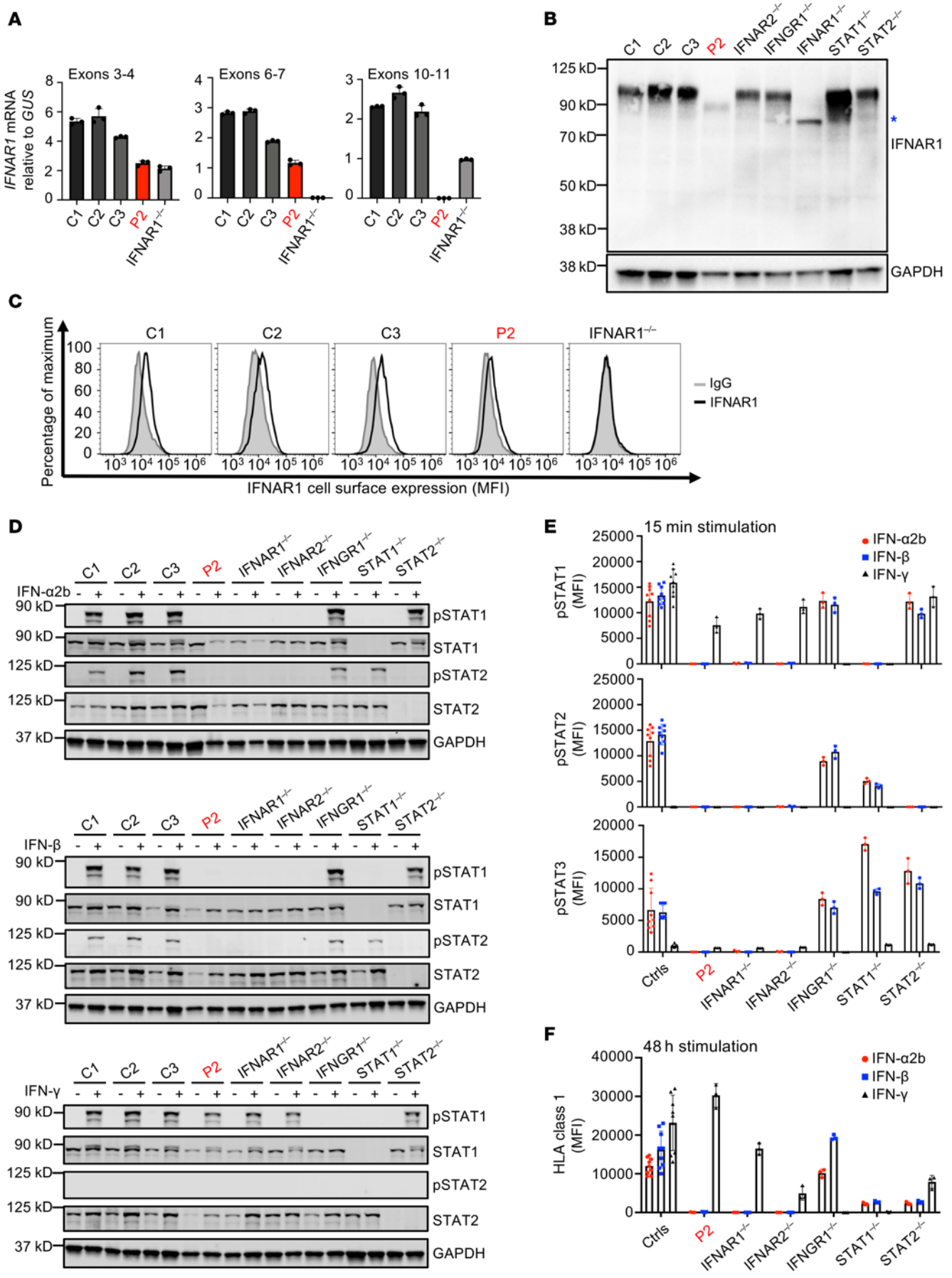

J Clin Invest. 2021;131(1):e139980 https://doi.org/10.1172/JCI139980

Figure 4. Patient SV40-fibroblasts express a truncated IFNAR1 and do not respond to IFN-α/β. (**A**) *IFNAR1* mRNA levels in SV40-fibroblasts from 3 healthy controls (C1, C2, C3), P2, and the previously reported p.V225fs IFNAR1$^{-/-}$ patient; *GUS* was used as an expression control. Mean values and SD from 3 independent experiments, each with technical duplicates, are shown. (**B**) WB for IFNAR1 in SV40-fibroblasts from 3 healthy controls (C1, C2, C3), P2, and other patients with autosomal recessive (AR) complete deficiencies of the IFN signaling pathways (IFNAR1$^{-/-}$, IFNAR2$^{-/-}$, IFNGR1$^{-/-}$, STAT1$^{-/-}$, STAT2$^{-/-}$). A truncated form of IFNAR1 was observed in the cells from the previously reported IFNAR1$^{-/-}$ patient, as indicated by the blue asterisk. An antibody recognizing the N-terminal part of the IFNAR1 protein was used. GAPDH was used as a loading control. (**C**) Extracellular FACS staining of IFNAR1 in SV40-fibroblasts from 3 healthy controls (C1, C2, C3), P2, and the previously reported IFNAR1$^{-/-}$ patient. Cells were not permeabilized. An antibody recognizing the N-terminal part of the protein was used. (**D**) WB of p-STAT1, p-STAT2, and unphosphorylated STAT1 and STAT2 in SV40-fibroblasts stimulated with 1000 U/mL IFN-α2b, IFN-β, or IFN-γ for 15 minutes. The cells used were from 3 healthy controls (C1, C2, C3), P2, and IFNAR1$^{-/-}$, IFNAR2$^{-/-}$, IFNGR1$^{-/-}$, STAT1$^{-/-}$, and STAT2$^{-/-}$ patients. GAPDH was used as a loading control. The results shown in **B**–**D** are representative of 3 independent experiments. (**E**) MFI following the intracellular FACS staining of p-STAT1, p-STAT2, and p-STAT3 in SV40-fibroblasts stimulated with 1000 U/mL IFN-α2b, IFN-β, or IFN-γ for 15 minutes. The values presented are after subtraction of the nonstimulated condition's value. (**F**) MFI after extracellular FACS staining of HLA class I in SV40-fibroblasts stimulated with 1000 U/mL IFN-α2b, IFN-β, or IFN-γ for 48 hours. MFI (and SD) values from 3 independent experiments are shown in **E** and **F**.

various viruses, including vesicular stomatitis virus (VSV), measles virus, and HSV-1 (9, 42, 54). When SV40-fibroblasts from P2 were infected with VSV, enterovirus 71 (EV71), or HSV-1, higher levels of viral replication were observed than in healthy control cells, as previously reported for a patient with AR complete TLR3 deficiency, a patient with AR complete STAT1 deficiency, and a previously reported IFNAR1-deficient patient (9, 24, 42). Furthermore, prior treatment with IFN-α2b or IFN-β did not rescue these viral phenotypes in the fibroblasts of the IFNAR1-deficient patient, whereas such pretreatment fully protected cells from healthy controls and the TLR3-deficient patient (Figure 7, A–F; and Supplemental Figure 7A). Consistent with our previous findings (11, 24, 42), neither IFN-α2b nor IFN-β fully rescued these viral phenotypes in STAT1-deficient fibroblasts, although some level of protection was observed relative to IFNAR1-deficient cells assessed in the same conditions (Figure 7, A, B, and D–F). Consistent with previous reports that IFN-γ displays some antiviral activity in some in vitro experimental conditions (58–62), IFN-γ pretreatment partially rescued the VSV replication phenotype in IFNAR1-deficient patient fibroblasts, whereas this treatment did not rescue this viral phenotype in STAT1-deficient cells (Figure 7, A and C). These results suggest that, in patients with inherited IFNAR1 deficiency, intact IFN-γ signaling may perhaps, to some extent, contribute to protection against some viral infections. We did not study the protective effect of IFN-λ in human dermal fibroblasts, owing to the lack of IFNLR expression in this cell type (23, 40, 63). Finally, the expression of exogenous WT IFNAR1 rescued the HSV-1 replication phenotype in P2's fibroblasts, to the levels of healthy control cells (Supplemental Figure 7, B and C). Therefore, consistent with previous findings with other viruses (42), inherited IFNAR1 deficiency also renders fibroblasts highly susceptible to HSV-1.

Discussion

We report a child with a distinctive form of AR complete IFNAR1 deficiency, with cell surface expression of a nonfunctional IFNAR1. AR complete IFNAR1 deficiency has been reported as a genetic cause of severe adverse reactions to measles or yellow fever live attenuated vaccines (LAVs) in 2 unrelated children (42, 64). Unlike the *IFNAR1* mutations reported in those patients, which led to a loss of cell surface IFNAR1 expression, the large homozygous deletion in the *IFNAR1* gene found in the patients studied here led to the expression of a C-terminally truncated IFNAR1 protein that was nevertheless expressed at the cell membrane. The truncated IFNAR1 protein can presumably bind IFN-α and -β, as the extracellular domain is intact (65). However, this mutant protein displays a loss of function due to its inability to interact with TYK2, to induce STAT phosphorylation, and to activate the JAK-STAT–dependent antiviral IFN-α/β signaling pathway. IFNAR1 is 1 of the 2 subunits of the receptor of the 17 subtypes of human type I IFNs, comprising 13 IFN-α subtypes, 1 IFN-β, 1 IFN-ω, 1 IFN-ε, and 1 IFN-κ (40). IFN-ω, IFN-ε, and IFN-κ are selectively produced by leukocytes, cells of the female reproductive tract, and keratinocytes, respectively, whereas IFN-α and IFN-β are produced by a broad range of human cells (66–69). It is probable, but not proven, that this C-terminal truncation of IFNAR1 impairs the signaling of all subtypes of IFN type I, in more than 400 different human cell types (70–72). Nevertheless, this truncation clearly completely abolished the induction of STAT1, STAT2, and STAT3 phosphorylation, and induction of the ISGs tested, upon stimulation with IFN-α2b and -β in dermal fibroblasts and EBV-B cells. GW transcriptomic responses to IFN-α2b were also completely abolished in the primary fibroblasts of the patients. Moreover, the viral phenotypes of patient fibroblasts were not rescued by treatment with IFN-α2b or -β, further confirming a complete IFNAR1 deficiency. Complete cytokine receptor deficiency due to the expression at the cell surface of a nonfunctional receptor has already been documented for IFNGR1, IFNGR2, IL-17RA, IL10-RA, IL10-RB, IL-6ST, and IL-12RB1, with mutations impairing cytokine binding (53, 73–79). By contrast to these previous observations, the mutant IFNAR1 reported here is loss-of-function owing to the absence of most of its intracellular domain, abolishing its signaling activity. The detection of IFNAR1 at the cell surface is not, therefore, sufficient to exclude a diagnosis of IFNAR1 deficiency.

The index case, with a distinctive form of AR complete IFNAR1 deficiency, suffered from HSE. The cellular phenotype of enhanced viral susceptibility due to IFNAR1 deficiency provides a plausible mechanism of disease pathogenesis for HSE and other documented or suspected viral diseases in the 2 IFNAR1-deficient relatives (P1, P2) and perhaps in P3 (from whom no genetic material is available), through the impairment of cell-intrinsic type I IFN immunity in organ-specific cells, hematopoietic cells, or both. Following on from previous findings of single-gene inborn errors of TLR3- and IFN-mediated immunity underlying childhood forebrain HSE in some children, we provide additional evidence that monogenic inborn errors of TLR3 and IFN immunity can result in HSE. This finding highlights the crucial role of IFNAR1/IFNAR2-mediated

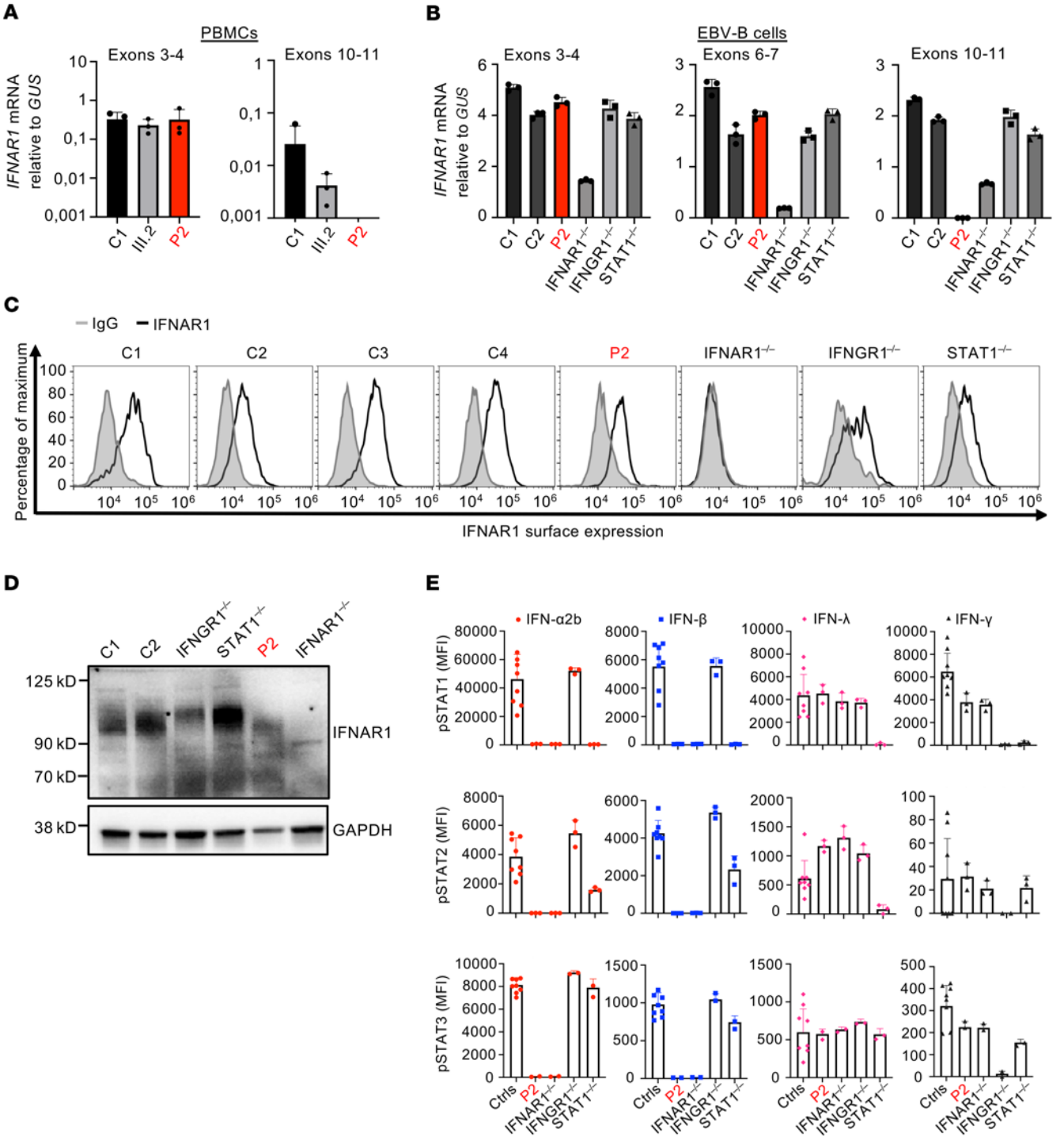

Figure 5. Patient EBV-B cells express a truncated IFNAR1 and do not respond to IFN-α/β. (**A**) *IFNAR1* mRNA levels, in PBMCs from 1 healthy control, P1's father (III.2), and P2. The *GUS* housekeeping gene was used as an expression control. Mean (and SD) values from 3 independent experiments, each with technical duplicates, are shown. (**B**) *IFNAR1* mRNA levels in EBV-B cells from 2 healthy controls, P2, and previously reported IFNAR1$^{-/-}$, IFNGR1$^{-/-}$, and STAT1$^{-/-}$ patients; the housekeeping gene *GUS* was used as an expression control. Mean (and SD) values from 3 independent experiments, each with technical duplicates, are shown. (**C**) Extracellular FACS staining of IFNAR1 in EBV-B cells from 4 healthy controls, P2, and IFNAR1$^{-/-}$, IFNGR1$^{-/-}$, and STAT1$^{-/-}$ patients. Cells were not permeabilized. An antibody recognizing the N-terminal part of the protein was used. The results shown are representative of 3 independent experiments. (**D**) WB of IFNAR1 in EBV-B cells from 2 healthy controls (C1, C2), P2, and IFNAR1$^{-/-}$, IFNGR1$^{-/-}$, and STAT1$^{-/-}$ patients. An antibody recognizing the N-terminal side of the protein was used. GAPDH was used as a loading control. A representative blot from 3 independent experiments is shown. (**E**) MFI after intracellular FACS staining of p-STAT1, p-STAT2, and p-STAT3, in EBV-B cells stimulated with 1000 U/mL IFN-α2b, IFN-β, IFN-λ, or IFN-γ for 15 minutes. The cells used were from 3 healthy controls (C1, C2, C3), P2, and IFNAR1$^{-/-}$, IFNGR1$^{-/-}$, and STAT1$^{-/-}$ patients. MFI (and SD) values from 3 independent experiments are shown.

IFN-α/β immunity to HSV-1 infection in the CNS. A previously reported patient with AR complete STAT1 deficiency (impairing type I, II, and III IFN signaling) developed HSE, in addition to other infectious phenotypes (24). It has also been suggested that AR complete deficiencies of other antiviral IFN pathway genes (*TYK2* and *IRF9*) may be related to the development of HSV-1 meningoencephalitis in 2 other unrelated children (refs. 80, 81, and our unpublished observations) (Table 1). By contrast, the 32 reported patients with IL-10RB deficiency (impairing type III IFN signaling) did not suffer from HSE, although this may be because most had died or undergone hematopoietic stem cell transplantation before exposure to HSV-1 (77). Consistent with our findings, IFNAR1/IFNAR2 was expressed at detectable levels in iPSC-derived cortical neurons, whereas IFNLR1 was not, and enhanced susceptibility to HSV-1 was rescued by pretreatment with IFN-α/β, but not IFN-λ, in TLR3-deficient iPSC-derived cortical neurons (15, 82). This phenotype contrasts with our recent observation that IFN-λ can rescue TLR3 deficiency in iPSC-derived pulmonary epithelial cells (23). We also showed that EBV-B cells from this patient and a previously reported IFNAR1-deficient patient responded normally to IFN-λ. At this stage, we cannot yet exclude the remote but finite possibility that other patients unresponsive to IFN-λ (response mediated via IL-10RB/IFNLR1) may suffer from HSE, with incomplete penetrance, as described for most of the previously reported single-gene inborn errors of the TLR3-IFN circuit (83). Nevertheless, the finding of AR IFNAR1 deficiency in an HSE patient provides proof of principle that type I IFN plays a nonredundant role in anti–HSV-1 immunity in the CNS. Inferred from our previous studies of TLR3 pathway deficiency underlying HSE (10–13, 18–21), the cellular basis of HSE pathogenesis due to IFNAR1 deficiency may involve an impairment of CNS cell-intrinsic immunity, although further investigations are required to confirm this. The findings reported here suggest that early treatment with commercially available IFN-β or IFN-α2, in addition to acyclovir, may be beneficial in patients with HSE whose cells respond to IFN-α/β.

IFNs were originally identified as antiviral cytokines (49, 50, 84). Mice with IFNAR1/2 deficiency are highly susceptible to various viral infections, including HSV-1 infection of the CNS (85–87). We report 2 human patients with IFNAR1 deficiency and documented or suspected severe viral diseases (documented HSE in P1; suspected other infections in P1 and P2) in natural conditions of infection — to our knowledge, the first such patients reported. P3 (genotype not confirmed), like previously reported patients with IFNAR1 or IFNAR2 deficiency, suffered from disease caused by LAVs (42, 88). Interestingly, unlike previously described HSE patients, P1 had suspected herpetic mucocutaneous lesions concomitant with HSE. Moreover, P2, also homozygous for the *IFNAR1* deletion, had suffered from 2 episodes of suspected HSV meningitis and 1 episode of suspected severe mumps virus infection, suggesting that AR IFNAR1 deficiency may also confer a predisposition to other severe viral infections. Consistently, AR deficiencies of other key molecules of the human type I IFN signaling pathway have been reported, each associated with different viral infections occurring in natural conditions or following vaccination with LAVs (Table 1) (24, 42, 54, 55, 81, 88–93). Nevertheless, with the exception of patients with AR STAT1 deficiency, who present a broad range of viral and nonviral infections (24, 54, 89, 92, 93), these patients suffer from a surprisingly narrow range of infections. The clinical penetrance of these deficiencies is clearly incomplete, but difficult to estimate, given the small number of patients with the various genetic defects and the sporadic nature of each infectious condition. The 2 previously reported patients with AR complete IFNAR1 deficiency suffered from severe adverse reactions to LAVs, but not HSE or other severe viral infections, although at least one IFNAR1-deficient patient had been exposed to HSV-1, as demonstrated by seropositivity for anti–HSV-1 antibodies (42). Conversely, the IFNAR1-deficient P1 reported here and one of the previously reported IFNAR1-deficient patients (42) had been vaccinated against MMR with no severe adverse reaction. The incomplete clinical penetrance and narrow viral phenotypes of human IFNAR1/IFNAR2 pathway deficiencies cannot currently be explained by residual IFN-α/β responses dependent on or independent of IFNAR1, as the experimental data reported here show a complete abolition of GW ISG induction in response to IFN-α2b, due to IFNAR1 deficiency, at least in fibroblasts. Other, type I IFN–independent, virus- and/or tissue-specific antiviral mechanisms may be crucial in some conditions (16, 17, 94, 95), and may, together with type I IFNs, constitute a first line of antiviral defense in humans.

Methods

Identifications of copy number variants. Whole-exome sequencing (WES) was performed as described in Supplemental Methods. Rare homozygous deletions were identified with the HMZDelFinder tool in a data set composed of the exome of the patient and 100 other exomes with similar coverage profiles for coding sequences. *IFNAR1* deletion ranked first based on *z* score, indicating a high degree of confidence in its being a true positive.

Cells. PBMCs were isolated by Ficoll-Paque density gradient (GE Life Science) centrifugation. Primary fibroblasts, SV40-immortalized dermal fibroblasts, and Vero E6 cells were maintained in DMEM (Thermo Fisher Scientific) supplemented with 10% FBS (Thermo Fisher Scientific). EBV-B cells were maintained in RPMI medium (Thermo Fisher Scientific) supplemented with 10% FBS.

Plasmids. The cDNA of *IFNAR1* was inserted into the pGEMT cloning vector (Promega). Site-directed mutagenesis was performed to obtain the indicated mutant constructs. All *IFNAR1* constructs were then subcloned into pCAGGS for overexpression studies. For lentiviral vector production, lentiviral vector transfer plasmid pCH_EF1a_IFNaR1_IRES_Bsd was generated as previously described (42). All constructs were resequenced to ensure that no adventitious mutations were generated during the cloning process.

IFNAR1 overexpression by plasmid transfection and generation of stably reconstituted cell lines. The pCAGGS-*IFNAR1* plasmid was used to transfect HEK293T cells, HeLa cells, or SV40-fibroblasts, by incubation for 24 hours or 48 hours, in the presence of X-tremeGene 9 transfection reagent (Sigma-Aldrich). We used 1 μg of plasmid to transfect 0.5×10^6 cells. For stable transduction of the patient fibroblasts with WT *IFNAR1*, HIV-based vectors were generated as previously described (42) and used to transduce SV40-fibroblasts in a serial dilution series. Cells were cultured and

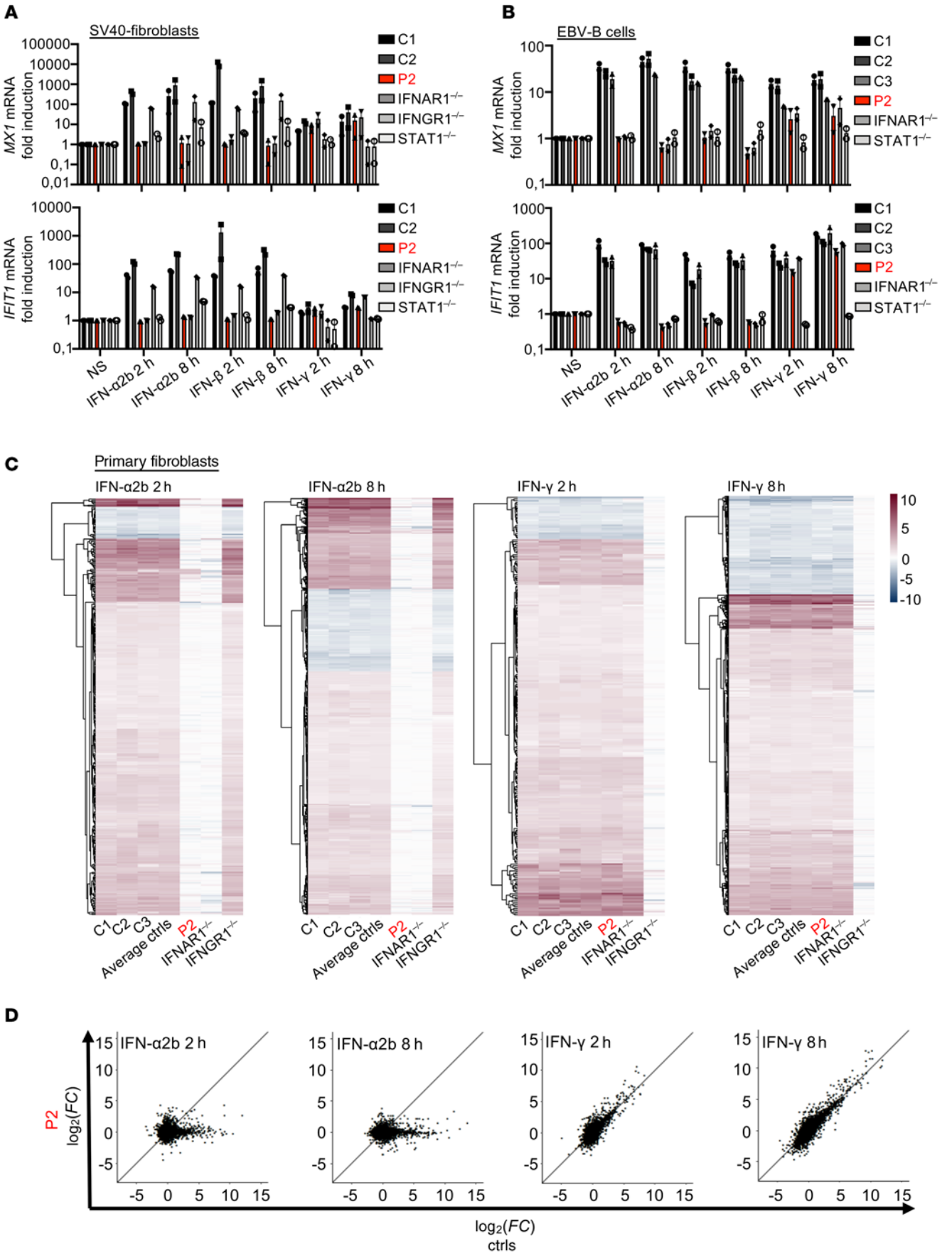
A
SV40-fibroblasts
MX1 mRNA fold induction
IFIT1 mRNA fold induction
C1
C2
P2
IFNAR1−/−
IFNGR1−/−
STAT1−/−
B
EBV-B cells
C3
NS
IFN-α2b 2 h
IFN-α2b 8 h
IFN-β 2 h
IFN-β 8 h
IFN-γ 2 h
IFN-γ 8 h
C
Primary fibroblasts
Average ctrls
D
log2(FC)
ctrls

Figure 6. Abolition of the induction of ISGs in response to IFN-α/β in patient fibroblasts and EBV-B cells. (**A**) Fold change in *IFIT1* and *MX1* mRNA levels after the stimulation, with IFN-α2b, IFN-β, or IFN-γ, of SV40-fibroblasts from 2 healthy controls (C1, C2), P2, and IFNAR1$^{-/-}$, IFNGR1$^{-/-}$, and STAT1$^{-/-}$ patients for 2 hours or 8 hours. The *GUS* housekeeping gene was used as an expression control. Mean and SD values from 3 independent experiments are shown. (**B**) Fold change in *IFIT1* and *MX1* mRNA levels after the stimulation, with IFN-α2b, IFN-β, or IFN-γ, of EBV-B cells from 3 healthy controls (C1, C2, C3), P2, and the IFNAR1$^{-/-}$ and STAT1$^{-/-}$ patients for 2 hours or 8 hours. The housekeeping gene *GUS* was used as an expression control. Mean and SD values from 3 independent experiments are shown. (**C**) Heatmaps of genes differentially expressed after 2 or 8 hours of stimulation with IFN-α2b or IFN-γ, in primary fibroblasts from 3 healthy controls (C1, C2, C3), P2, the IFNAR1$^{-/-}$ p.V225fs patient, and an IFNGR1$^{-/-}$ patient. For each set of conditions, we show the genes significantly differentially expressed with respect to the control group, i.e., with a $|\log_2(\text{fold change [FC]})| > 1$ and $P < 0.05$ after Benjamini-Hochberg correction, and genes with a $|\Delta\log_2(\text{FC})| > 1$ between the control group and the IFNAR1$^{-/-}$ patient or the IFNGR1$^{-/-}$ patient after stimulation with IFN-α2b and IFN-γ, respectively. The gradient from blue to red represents increasing $\log_2$(FC). Genes are clustered by Euclidean distance. (**D**) Scatterplots of $\log_2$(FC) in RNA-Seq–quantified gene expression following stimulation with IFN-α2b or IFN-γ for 2 or 8 hours, in primary fibroblasts from P2 versus 3 healthy controls (C1, C2, and C3). Each dot represents a single gene.

subjected to blasticidin selection (5 μg/mL). IFNAR1 expression was corroborated by Western blotting.

TOPO cloning. RNA was extracted from the cells of P2 and a homozygous healthy control, and the corresponding cDNA was generated with the High-Capacity RNA-to-cDNA kit (Thermo Fisher Scientific). Specific primers were used to amplify IFNAR1 cDNA by PCR, from the start of exon 10 until the 3′-UTR. The primers used were: forward, GCTGCGAAAGTCTTCTTGAGATGC; and reverse, CCATGTAAGGGTAGATACTGTGATGTG. PCR products were then purified and ligated into a pCR4-TOPO vector and used to transform DH5α competent cells (Thermo Fisher Scientific). The bacteria were plated on LB agar plates containing 100 μg/mL ampicillin, which were incubated at 37°C overnight. Single colonies were then picked, and the inserted cDNA was amplified and sequenced with the M13 forward and reverse primers.

VirScan. VirScan assay was used to assess antibody responses to microbial species on the basis of stringent cutoff values, as previously described (96).

RNA-Seq. Total RNA was extracted from primary fibroblasts from patients or healthy controls with the miRNeasy Mini Kit (Zymo Research), and treated with DNase (Zymo Research) to remove residual gDNA. Quality controls were performed, and all RNA samples were of good quality (RNA integrity number >8). RNA-Seq libraries were prepared with the Illumina RiboZero TruSeq Stranded Total RNA Library Prep Kit and sequenced on the Illumina NextSeq platform in the 150-nt, paired-end configuration. Each library was sequenced twice. The sequencing data were then analyzed as described in Supplemental Methods. The raw sequencing data were deposited in the NCBI's Gene Expression Omnibus database (GEO GSE157948).

Western blotting. Fibroblasts or EBV-B cells were left untreated or were treated with IFN-α2b (Schering), IFN-β (PBL Assay Science), or IFN-γ (Imukin, Boehringer Ingelheim) for the specified times before lysis. Cells were lysed in NP-40 lysis buffer (280 mM NaCl, 50 mM Tris [pH 8], 0.2 mM EDTA, 2 mM EGTA, 10% glycerol, 0.5% NP-40) supplemented with 1 mM DTT, PhosSTOP (Roche), and cOmplete Protease Inhibitor Cocktail (Roche). The protein lysate was subjected to SDS-PAGE, and the bands obtained were transferred to a nitrocellulose membrane, which was probed with unconjugated primary antibodies and secondary antibodies adapted for LI-COR. An anti-GAPDH antibody (Santa Cruz Biotechnology) was used as a loading control. For endogenous IFNAR1, we used an antibody recognizing the N-terminus of the IFNAR1 protein at a dilution of 1:1000 (64G12 custom antibody), whereas, for the protein overproduced following transfection, we used a polyclonal anti-IFNAR1 antibody recognizing the C-terminus of IFNAR1 (ab45172, Abcam). Antibodies against STAT1 (610116, BD Biosciences), p-STAT1 (562070, BD Biosciences), STAT2 (07-140, EMB), p-STAT2 (4441, Cell Signaling Technology), STAT3 (catalog 610189, BD Biosciences), p-STAT3 (562072, BD Biosciences), TYK2 (C8, sc-5271, Santa Cruz Biotechnology), and GAPDH (sc-47724, Santa Cruz Biotechnology) were purchased from commercial suppliers. The membrane was incubated overnight at 4°C with the primary antibodies. SuperSignal West Pico Chemiluminescent substrate (Thermo Fisher Scientific) was used to visualize HRP activity, and this signal was detected with an Amersham Imager 600 (GE Life Sciences). See complete unedited blots in the supplemental material.

Flow cytometry. For measurement of the cell surface expression of IFNAR1, control or patient EBV-B cells or SV40-fibroblasts were plated in 96-well plates, at a density of 5×10^5 cells per well, and surface-stained with either purified mouse anti-IFNAR1 (AA3 custom antibody) or PE-conjugated mouse anti-IFNAR2 (21385-3, PBL Assay Science) antibody. Cells stained with AA3 were then washed once with PBS and incubated with a biotinylated rat anti-mouse secondary antibody (Thermo Fisher Scientific) for 30 minutes, before being washed once with PBS and incubated for 30 minutes with PE-conjugated streptavidin (Thermo Fisher Scientific). The cells were then washed twice with PBS and analyzed by flow cytometry. Data were acquired on a Gallios flow cytometer (Beckman Coulter), and the results were analyzed with FlowJo software (Tree Star).

Real-time qPCR. RNA was isolated from PBMCs, EBV-B cells, fibroblasts, or HEK293T cells with and without plasmid transfection, with a kit, according to the manufacturer's protocol (Zymo Research), and treated with DNase (Zymo Research). Reverse transcription was performed with random hexamers and the SuperScript III reverse strand synthesis kit, according to the manufacturer's instructions (Thermo Fisher Scientific). Real-time qPCR was performed with Applied Biosystems TaqMan assays for *IFNAR1*, and the β-glucuronidase (GUS) housekeeping gene for normalization. Results are expressed according to the ΔΔCt method, as described by the kit manufacturer.

Viral assays. For VSV infection, 1.25×10^5 SV40-fibroblasts per well were added to 24-well plates and infected with VSV (Indiana strain), at an MOI of 3, in DMEM supplemented with 2% FCS. After incubation for 2 hours, the cells were washed and incubated in 1 mL of medium. Cells and supernatants were obtained at various time points and frozen. VSV titers were determined by calculation of the 50% end point ($TCID_{50}$), as described by Reed and Muench (97), after the inoculation of Vero cell cultures in 96-well plates. For HSV-1 (KOS strain, ATCC) and EV71 (ATCC) infection, 1.25×10^5 SV40-fibroblasts per well were added to 24-well plates and

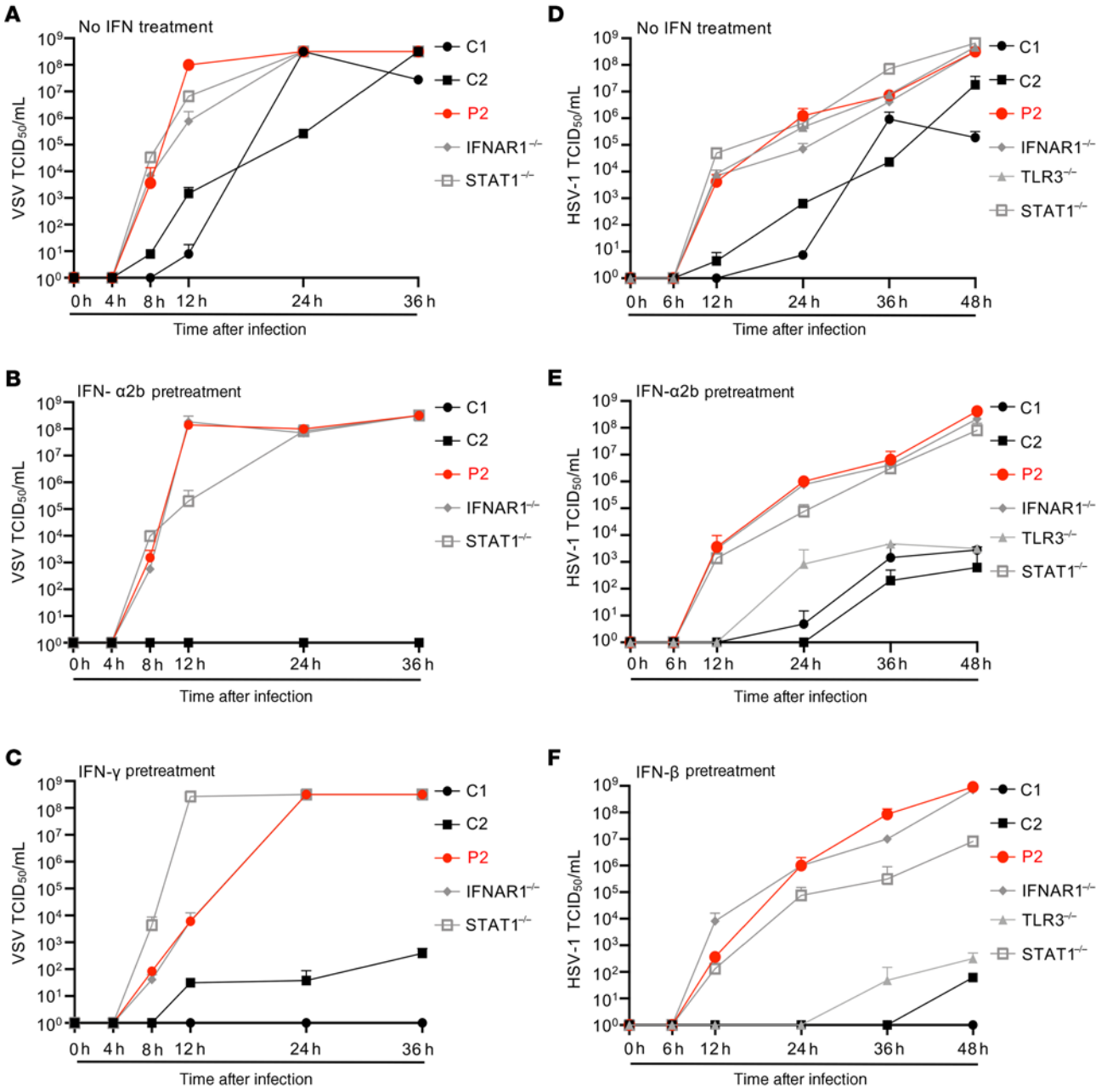

Figure 7. Enhanced viral replication in patient SV40-fibroblasts in the presence and absence of treatment with IFN-α2b or IFN-β. (**A**–**C**) VSV replication, quantified by the $TCID_{50}$ method, in SV40-fibroblasts from 2 healthy controls (C1, C2), P2, and IFNAR1$^{-/-}$ and STAT1$^{-/-}$ patients, 4, 8, 12, 24, and 36 hours after infection with VSV at an MOI of 3, without (**A**) or with prior treatment with 1000 IU IFN-α2b (**B**) or IFN-γ (**C**) for 16 hours. Mean values ± SD from 3 independent experiments, each including biological triplicates, are shown. (**D**–**F**) HSV-1 replication, quantified by the $TCID_{50}$ method, in SV40-fibroblasts from 2 healthy controls, P2, and IFNAR1$^{-/-}$, TLR3$^{-/-}$, and STAT1$^{-/-}$ patients, 6, 12, 24, 36, and 48 hours after infection with HSV-1 at an MOI of 1, without (**D**) or with prior treatment with 1000 IU IFN-α2b (**E**) or IFN-β (**F**) for 16 hours. Mean values ± SD from 3 independent experiments are shown (**A**–**F**). Biological triplicates were included in each experiment for VSV infection, with duplicates for HSV-1 infection.

infected with HSV-1 or EV71, at a MOI of 0.01 or 10, respectively, in DMEM supplemented with 2% FCS. After 2 hours, the cells were washed and incubated in 500 μL of medium. Cells and supernatants were collected at various time points and frozen. HSV-1 titers were determined by calculation of the $TCID_{50}$, as described by Reed and Muench, after the inoculation of Vero cell cultures in 96-well plates.

Study approval. The patients and the other members of their family were living in Palestinian territory, and were followed up in Israel. Informed consent was obtained in their country of follow-up, in accordance with local regulations and the requirements for institutional review board approval from Rockefeller University and INSERM. Experiments were conducted in the United States and France, in accordance with local regulations and with the approval of the institutional review board of Rockefeller University and INSERM, respectively. Detailed patient clinical information is provided in Supplemental Methods.

Table 1. Clinical phenotypes of patients with autosomal recessive genetic defects of the type I IFN pathway

Gene	Defect	Number of patients	Age at first infection	Viral phenotype	Mycobacterial phenotype	Other infection	Ref.
IFNAR1	Complete	2	9 yr, 12 yr	Severe reaction to MMR (disseminated measles with meningoencephalitis) or YEL-AVD	NR	NR	42
	Complete	2	6 mo, 13 mo	HSE (P1); HSV meningitis? deafness after mumps? (P2), death after MMR (P3, not genotyped)	NR	NR	This paper
IFNAR2	Complete	1	13 mo	Severe reaction to MMR (meningoencephalitis)	NR	NR	88
IFNAR1 and IFNGR2	Partial	1	2 mo	CMV viremia	MSMD	Bacterial infection	90
TYK2	Complete	1	12 mo	Molluscum contagiosum, herpes simplex infection of skin and mucosa; PIV3 pneumonia	MSMD	Bacterial and fungal infection	98
		7	2 mo to 13 yr	Recurrent VZV cutaneous infections; other cutaneous viral infections; herpes meningitis +/– encephalitis?	MSMD	Bacterial and fungal infection	80
		1	5 yr	NR	NR	Bacterial infection	99
		1	7 mo	HSV gingivostomatitis, aseptic meningitis (virus not identified), severe chicken pox	MSMD	NR	100
	Partial	11	1 yr to 40 yr	NR	TB, MSMD	CMC	101
		2	13 yr, 15 yr	EBV-associated B cell lymphoma	NR	NR	102
JAK1	Partial	1	1 yr	NR	MSMD	NR	103
STAT1	Complete	2	2 mo, 3 mo	P1 died of recurrent HSE; P2 died of viral illness	MSMD	NR	24
		1	3 mo	Fulminant EBV infection	MSMD	NR	54
		1	10 mo	Severe pulmonary CMV infection	MSMD	NR	92
		1	8 mo	Severe reaction to MMR vaccination (encephalitis), multisystem inflammatory disorder related to HHV6 infection	NR	NR	104
	Partial	2	2 yr	Viral diseases due to CMV, VZV, HSV	NR	Salmonella	105
		2	1 mo, 6 yr	Disseminated chicken pox	MSMD	Fungal infection	106
		1	14 yr	NR	MSMD	NR	93
STAT2	Complete	5	1 mo to 6 yr	Severe reaction to MMR (pneumonitis, hepatitis); severe viral disease of unclear origin	NR	NR	55
		2	12 mo, 13 mo	Severe reaction to MMR (meningoencephalitis, opsoclonus-myoclonus)	NR	NR	107
		2	2 mo, 6 mo	Recurrent cutaneous HSV infections; severe reaction to MMR; recurrent severe viral infection (VZV, EBV, enterovirus, IAV, adenovirus, etc.)	NR	NR	62
IRF9	Complete	1	1 yr	IAV pneumonitis, biliary perforation after MMR	NR	NR	108
		2	1 yr	Severe pulmonary IBV infection; biliary perforation after MMR; HSE and death after YFV (sibling with suspected IRF9 deficiency, not genotyped)	NR	NR	81
IRF7	Complete	1	2.5 yr	IAV pneumonitis	NR	NR	91

CMC, chronic mucocutaneous candidiasis; CMV, cytomegalovirus; EBV, Epstein-Barr virus; HHV6, human herpesvirus 6; HSE, herpes simplex encephalitis; IAV, influenza A virus; IBV, influenza B virus; MMR, measles, mumps, and rubella; MSMD, Mendelian susceptibility to mycobacterial disease; NR, not reported; PIV3, parainfluenza virus type 3; TB, tuberculosis; YEL-AVD, yellow fever vaccine–associated viscerotropic disease; YFV, yellow fever vaccine; VZV, varicella zoster virus.

Author contributions

PB identified the mutation. PB, JR, LL, and JC performed the experiments. PB, JM, PZ, YS, B. Bigio, B. Boisson, AC, and LA analyzed the data. OA, SS, and RS recruited and treated the patients. MH, NH, RL, EJGR, YSL, SB, MA, VB, RG, ZL, SP, IM, FR, NM, and TK helped in the design of the study and performed some of the experiments. JB, QZ, and EJ helped in the design of the study and data analysis. JLC and SYZ supervised the study. PB, JLC, and SYZ wrote the manuscript. All authors contributed to and edited the manuscript.

Acknowledgments

We warmly thank our patients and their families. We thank the members of both branches of the Laboratory of Human Genetics of Infectious Diseases for helpful discussions; Tatiana Kochetkov for technical assistance; Dominick Papandrea, Cécile Patissier, and Yelena Nemirovskaya for administrative assistance; Mahbuba Rahman, Fatima Al Ali, and Manar Ata for help with VirScan data analysis; and Stephen Elledge (Brigham and Women's Hospital, Harvard Medical School) for providing the VirScan phage library that was used in this study for antibody profiling in the patient and controls. This work was conducted in the 2 branches of the Laboratory of Human Genetics of Infectious Diseases, and was funded in part by the National Center for Advancing Translational Sciences/NIH/Clinical and Translational Science Award program (grant UL1TR001866); NIH grants R01AI088364, R01NS072381, and R21AI151663; National Vaccine Program Office of the US

Department of Health and Human Services grant VSRNV000006; grants from the Integrative Biology of Emerging Infectious Diseases Laboratory of Excellence (ANR-10-LABX-62-IBEID) and the French National Research Agency (ANR) under the "Investments for the future" program (ANR-10-IAHU-01); ANR grants IEIHSEER (ANR-14-CE14-0008-01), SEAeHostFactors (ANR-18-CE15-0020-02), and CNSVIRGEN (ANR-19-CE15-0009-01); the French Foundation for Medical Research (FRM) (EQU201903007798); the Qatar National Research Fund (NPRP9-251-3-045); Rockefeller University; INSERM; University of Paris; and the St. Giles Foundation. PB was supported by the FRM (EA20170638020) and the MD-PhD program of the Imagine Institute (with the support of the Fondation Bettencourt-Schueller). JR was supported by the INSERM PhD program ("poste d'accueil Inserm"). JM was supported by ANR grants BURULIGEN (ANR-12-BSV3-0013-01) and MYCOPARADOX (ANR-16-CE12-0023). IM is a senior clinical investigator at the Fonds Wetenschappelijk Onderzoek (FWO) Vlaanderen and is supported by FWO grant G0C8517N.

Address correspondence to: Shen-Ying Zhang, Rockefeller University, 1230 York Avenue, New York, New York 10065, USA. Phone: 212.327.7333; Email: shzh289@rockefeller.edu.

1. Abel L, et al. Age-dependent Mendelian predisposition to herpes simplex virus type 1 encephalitis in childhood. *J Pediatr*. 2010;157(4):623–629.
2. Whitley RJ. Herpes simplex virus infections of the central nervous system. *Continuum (Minneap Minn)*. 2015;21(6 Neuroinfectious Disease):1704–1713.
3. Jmor F, Emsley HCA, Fischer M, Solomon T, Lewthwaite P. The incidence of acute encephalitis syndrome in Western industrialised and tropical countries. *Virol J*. 2008;5:134.
4. Jubelt B, Mihai C, Li TM, Veerapaneni P. Rhombencephalitis / brainstem encephalitis. *Curr Neurol Neurosci Rep*. 2011;11(6):543–552.
5. Whitley RJ, et al. Vidarabine versus acyclovir therapy in herpes simplex encephalitis. *N Engl J Med*. 1986;314(3):144–149.
6. Arciniegas DB, Anderson CA. Viral encephalitis: neuropsychiatric and neurobehavioral aspects. *Curr Psychiatry Rep*. 2004;6(5):372–379.
7. Stahl JP, Mailles A. Herpes simplex virus encephalitis update [published online March 27, 2019]. *Curr Opin Infect Dis*. https://doi.org/10.1097/QCO.0000000000000554.
8. Mailles A, et al. Long-term outcome of patients presenting with acute infectious encephalitis of various causes in France. *Clin Infect Dis*. 2012;54(10):1455–1464.
9. Zhang SY, et al. TLR3 deficiency in patients with herpes simplex encephalitis. *Science*. 2007;317(5844):1522–1527.
10. Casrouge A, et al. Herpes simplex virus encephalitis in human UNC-93B deficiency. *Science*. 2006;314(5797):308–312.
11. Guo Y, et al. Herpes simplex virus encephalitis in a patient with complete TLR3 deficiency: TLR3 is otherwise redundant in protective immunity. *J Exp Med*. 2011;208(10):2083–2098.
12. Zhang SY, Casanova JL. Inborn errors underlying herpes simplex encephalitis: from TLR3 to IRF3. *J Exp Med*. 2015;212(9):1342–1343.
13. Herman M, et al. Heterozygous TBK1 mutations impair TLR3 immunity and underlie herpes simplex encephalitis of childhood. *J Exp Med*. 2012;209(9):1567–1582.
14. Zimmer B, et al. Human iPSC-derived trigeminal neurons lack constitutive TLR3-dependent immunity that protects cortical neurons from HSV-1 infection. *Proc Natl Acad Sci U S A*. 2018;115(37):E8775–E8782.
15. Lafaille FG, et al. Impaired intrinsic immunity to HSV-1 in human iPSC-derived TLR3-deficient CNS cells. *Nature*. 2012;491(7426):769–773.
16. Lafaille FG, et al. Human SNORA31 variations impair cortical neuron-intrinsic immunity to HSV-1 and underlie herpes simplex encephalitis. *Nat Med*. 2019;25(12):1873–1884.
17. Zhang SY, et al. Inborn errors of RNA lariat metabolism in humans with brainstem viral infection. *Cell*. 2018;172(5).
18. Zhang SY, Abel L, Casanova J-L. Mendelian predisposition to herpes simplex encephalitis. *Handb Clin Neurol*. 2013;112:1091–1097.
19. Sancho-Shimizu V, et al. Herpes simplex encephalitis in children with autosomal recessive and dominant TRIF deficiency. *J Clin Invest*. 2011;121(12):4889–4902.
20. Pérez de Diego R, et al. Human TRAF3 adaptor molecule deficiency leads to impaired Toll-like receptor 3 response and susceptibility to herpes simplex encephalitis. *Immunity*. 2010;33(3):400–411.
21. Audry M, et al. NEMO is a key component of NF-κB- and IRF-3-dependent TLR3-mediated immunity to herpes simplex virus. *J Allergy Clin Immunol*. 2011;128(3):610–617.
22. Zhang S-Y, et al. Human Toll-like receptor-dependent induction of interferons in protective immunity to viruses. *Immunol Rev*. 2007;220:225–236.
23. Lim HK, et al. Severe influenza pneumonitis in children with inherited TLR3 deficiency. *J Exp Med*. 2019;216(9):2038–2056.
24. Dupuis S, et al. Impaired response to interferon-alpha/beta and lethal viral disease in human STAT1 deficiency. *Nat Genet*. 2003;33(3):388–391.
25. Rosain J, et al. Mendelian susceptibility to mycobacterial disease: 2014-2018 update. *Immunol Cell Biol*. 2019;97(4):360–367.
26. Bustamante J. Mendelian susceptibility to mycobacterial disease: recent discoveries. *Hum Genet*. 2020;139(6–7):993–1000.
27. Zhang SY, et al. Inborn errors of interferon (IFN)-mediated immunity in humans: insights into the respective roles of IFN-alpha/beta, IFN-gamma, and IFN-lambda in host defense. *Immunol Rev*. 2008;226:29–40.
28. Zhang S-Y. Herpes simplex virus encephalitis of childhood: inborn errors of central nervous system cell-intrinsic immunity. *Hum Genet*. 2020;139(6–7):911–918.
29. Itan Y, et al. The mutation significance cutoff: gene-level thresholds for variant predictions. *Nat Methods*. 2016;13(2):109–110.
30. Itan Y, et al. The human gene damage index as a gene-level approach to prioritizing exome variants. *Proc Natl Acad Sci U S A*. 2015;112(44):13615–13620.
31. Gambin T, et al. Homozygous and hemizygous CNV detection from exome sequencing data in a Mendelian disease cohort. *Nucleic Acids Res*. 2017;45(4):1633–1648.
32. Lek M, et al. Analysis of protein-coding genetic variation in 60,706 humans. *Nature*. 2016;536(7616):285–291.
33. Karczewski KJ, et al. The mutational constraint spectrum quantified from variation in 141,456 humans. *Nature*. 2020;581(7809):434–443.
34. 1000 Genomes Project Consortium, et al. A global reference for human genetic variation. *Nature*. 2015;526(7571):68–74.
35. Sherry ST, Ward M, Sirotkin K. dbSNP-database for single nucleotide polymorphisms and other classes of minor genetic variation. *Genome Res*. 1999;9(8):677–679.
36. MacDonald JR, Ziman R, Yuen RKC, Feuk L, Scherer SW. The Database of Genomic Variants: a curated collection of structural variation in the human genome. *Nucleic Acids Res*. 2014;42(Database issue):D986–D992.
37. Collins RL, et al. A structural variation reference for medical and population genetics. *Nature*. 2020;581(7809):444–451.
38. Uzé G, Lutfalla G, Gresser I. Genetic transfer of a functional human interferon alpha receptor into mouse cells: cloning and expression of its cDNA. *Cell*. 1990;60(2):225–234.
39. Piehler J, Thomas C, Garcia KC, Schreiber G. Structural and dynamic determinants of type I interferon receptor assembly and their functional interpretation. *Immunol Rev*. 2012;250(1):317–334.
40. Lazear HM, Schoggins JW, Diamond MS. Shared and distinct functions of type I and type III interferons. *Immunity*. 2019;50(4):907–923.
41. Hardy MP, Owczarek CM, Jermiin LS, Ejdebäck M, Hertzog PJ. Characterization of the type I interferon locus and identification of novel genes. *Genomics*. 2004;84(2):331–345.
42. Hernandez N, et al. Inherited IFNAR1 deficiency in otherwise healthy patients with adverse reaction to measles and yellow fever live vaccines. *J Exp Med*. 2019;216(9):2057–2070.
43. Wallweber HJA, Tam C, Franke Y, Starovasnik MA, Lupardus PJ. Structural basis of recognition of interferon-α receptor by tyrosine kinase 2. *Nat Struct Mol Biol*. 2014;21(5):443–448.
44. Uhlen M, et al. A genome-wide transcriptomic

analysis of protein-coding genes in human blood cells. *Science*. 2019;366(6472):eaax9198.
45. Uhlén M, et al. Proteomics. Tissue-based map of the human proteome. *Science*. 2015;347(6220):1260419.
46. Wilmes S, et al. Receptor dimerization dynamics as a regulatory valve for plasticity of type I interferon signaling. *J Cell Biol*. 2015;209(4):579–593.
47. Russell-Harde D, et al. Role of the intracellular domain of the human type I interferon receptor 2 chain (IFNAR2c) in interferon signaling. Expression of IFNAR2c truncation mutants in U5A cells. *J Biol Chem*. 2000;275(31):23981–23985.
48. Yan H, et al. Phosphorylated interferon-alpha receptor 1 subunit (IFNaR1) acts as a docking site for the latent form of the 113 kDa STAT2 protein. *EMBO J*. 1996;15(5):1064–1074.
49. Isaacs A, Lindenmann J. Virus interference. I. The interferon. *Proc R Soc Lond B Biol Sci*. 1957;147(927):258–267.
50. Isaacs A, Lindenmann J, Valentine RC. Virus interference. II. Some properties of interferon. *Proc R Soc Lond B Biol Sci*. 1957;147(927):268–273.
51. Dupuis S, et al. Impairment of mycobacterial but not viral immunity by a germline human STAT1 mutation. *Science*. 2001;293(5528):300–303.
52. Lykke-Andersen S, Jensen TH. Nonsense-mediated mRNA decay: an intricate machinery that shapes transcriptomes. *Nat Rev Mol Cell Biol*. 2015;16(11):665–677.
53. Jouanguy E, et al. In a novel form of IFN-γ receptor 1 deficiency, cell surface receptors fail to bind IFN-gamma. *J Clin Invest*. 2000;105(10):1429–1436.
54. Chapgier A, et al. Human complete Stat-1 deficiency is associated with defective type I and II IFN responses in vitro but immunity to some low virulence viruses in vivo. *J Immunol*. 2006;176(8):5078–5083.
55. Hambleton S, et al. STAT2 deficiency and susceptibility to viral illness in humans. *Proc Natl Acad Sci U S A*. 2013;110(8):3053–3058.
56. Cheon H, et al. IFNβ-dependent increases in STAT1, STAT2, and IRF9 mediate resistance to viruses and DNA damage. *EMBO J*. 2013;32(20):2751–2763.
57. Stark GR, Cheon H, Wang Y. Responses to cytokines and interferons that depend upon JAKs and STATs. *Cold Spring Harb Perspect Biol*. 2018;10(1):a028555.
58. Wheelock EF. Interferon-like virus-inhibitor induced in human leukocytes by phytohemagglutinin. *Science*. 1965;149(3681):310–311.
59. Bouley DM, Kanangat S, Wire W, Rouse BT. Characterization of herpes simplex virus type-1 infection and herpetic stromal keratitis development in IFN-gamma knockout mice. *J Immunol*. 1995;155(8):3964–3971.
60. Yu Z, Manickan E, Rouse BT. Role of interferon-gamma in immunity to herpes simplex virus. *J Leukoc Biol*. 1996;60(4):528–532.
61. Pomeroy C, Delong D, Clabots C, Riciputi P, Filice GA. Role of interferon-gamma in murine cytomegalovirus infection. *J Lab Clin Med*. 1998;132(2):124–133.
62. Moens L, et al. A novel kindred with inherited STAT2 deficiency and severe viral illness. *J Allergy Clin Immunol*. 2017;139(6):1995-1997.
63. Lazear HM, Nice TJ, Diamond MS. Interferon-λ: immune functions at barrier surfaces and beyond. *Immunity*. 2015;43(1):15–28.
64. Pöyhönen L, Bustamante J, Casanova J-L, Jouanguy E, Zhang Q. Life-threatening infections due to live-attenuated vaccines: early manifestations of inborn errors of immunity. *J Clin Immunol*. 2019;39(4):376–390.
65. de Weerd NA, et al. A hot spot on interferon α/β receptor subunit 1 (IFNAR1) underpins its interaction with interferon-β and dictates signaling. *J Biol Chem*. 2017;292(18):7554–7565.
66. Pestka S, Krause CD, Walter MR. Interferons, interferon-like cytokines, and their receptors. *Immunol Rev*. 2004;202:8–32.
67. Hermant P, Francius C, Clotman F, Michiels T. IFN-ε is constitutively expressed by cells of the reproductive tract and is inefficiently secreted by fibroblasts and cell lines. *PLoS One*. 2013;8(8):e71320.
68. Scarponi C, et al. Analysis of IFN-kappa expression in pathologic skin conditions: downregulation in psoriasis and atopic dermatitis. *J Interferon Cytokine Res*. 2006;26(3):133–140.
69. Nardelli B, et al. Regulatory effect of IFN-kappa, a novel type I IFN, on cytokine production by cells of the innate immune system. *J Immunol*. 2002;169(9):4822–4830.
70. Vickaryous MK, Hall BK. Human cell type diversity, evolution, development, and classification with special reference to cells derived from the neural crest. *Biol Rev Camb Philos Soc*. 2006;81(3):425–455.
71. Sender R, Fuchs S, Milo R. Revised estimates for the number of human and bacteria cells in the body. *PLoS Biol*. 2016;14(8):e1002533.
72. Bianconi E, et al. An estimation of the number of cells in the human body. *Ann Hum Biol*. 2013;40(6):463–471.
73. Fieschi C, et al. A novel form of complete IL-12/IL-23 receptor beta1 deficiency with cell surface-expressed nonfunctional receptors. *Blood*. 2004;104(7):2095–2101.
74. Vogt G, et al. Gains of glycosylation comprise an unexpectedly large group of pathogenic mutations. *Nat Genet*. 2005;37(7):692–700.
75. Lévy R, et al. Genetic, immunological, and clinical features of patients with bacterial and fungal infections due to inherited IL-17RA deficiency. *Proc Natl Acad Sci U S A*. 2016;113(51):E8277–E8285.
76. Béziat V, et al. Dominant-negative mutations in human IL6ST underlie hyper-IgE syndrome. *J Exp Med*. 2020;217(6):e20191804.
77. Glocker EO, et al. Inflammatory bowel disease and mutations affecting the interleukin-10 receptor. *N Engl J Med*. 2009;361(21):2033–2045.
78. Schwerd T, et al. A biallelic mutation in IL6ST encoding the GP130 co-receptor causes immunodeficiency and craniosynostosis. *J Exp Med*. 2017;214(9):2547–2562.
79. Charbit-Henrion F, et al. Copy number variations and founder effect underlying complete IL-10Rβ deficiency in Portuguese kindreds. *PLoS One*. 2018;13(10):e0205826.
80. Kreins AY, et al. Human TYK2 deficiency: mycobacterial and viral infections without hyper-IgE syndrome. *J Exp Med*. 2015;212(10):1641–1662.
81. García-Morato MB, et al. Impaired control of multiple viral infections in a family with complete IRF9 deficiency. *J Allergy Clin Immunol*. 2019;144(1):309–312.e10.
82. Lafaille FG, et al. Deciphering human cell-autonomous anti-HSV-1 immunity in the central nervous system. *Front Immunol*. 2015;6:208.
83. Casanova JL. Severe infectious diseases of childhood as monogenic inborn errors of immunity. *Proc Natl Acad Sci U S A*. 2015;112(51):E7128–E7137.
84. Lindenmann J, Burke DC, Isaacs A. Studies on the production, mode of action and properties of interferon. *Br J Exp Pathol*. 1957;38(5):551–562.
85. Müller U, et al. Functional role of type I and type II interferons in antiviral defense. *Science*. 1994;264(5167):1918–1921.
86. Parker ZM, Murphy AA, Leib DA. Role of the DNA sensor STING in protection from lethal infection following corneal and intracerebral challenge with herpes simplex virus 1. *J Virol*. 2015;89(21):11080–11091.
87. Wang JP, et al. Role of specific innate immune responses in herpes simplex virus infection of the central nervous system. *J Virol*. 2012;86(4):2273–2281.
88. Duncan CJA, et al. Human IFNAR2 deficiency: lessons for antiviral immunity. *Sci Transl Med*. 2015;7(307):307ra154.
89. Boisson-Dupuis S, et al. Inborn errors of human STAT1: allelic heterogeneity governs the diversity of immunological and infectious phenotypes. *Curr Opin Immunol*. 2012;24(4):364–378.
90. Hoyos-Bachiloglu R, et al. A digenic human immunodeficiency characterized by IFNAR1 and IFNGR2 mutations. *J Clin Invest*. 2017;127(12):4415–4420.
91. Ciancanelli MJ, et al. Infectious disease. Life-threatening influenza and impaired interferon amplification in human IRF7 deficiency. *Science*. 2015;348(6233):448–453.
92. Vairo D, et al. Severe impairment of IFN-γ and IFN-α responses in cells of a patient with a novel STAT1 splicing mutation. *Blood*. 2011;118(7):1806–1817.
93. Kristensen IA, Veirum JE, Møller BK, Christiansen M. Novel STAT1 alleles in a patient with impaired resistance to mycobacteria. *J Clin Immunol*. 2011;31(2):265–271.
94. Ramoz N, et al. Mutations in two adjacent novel genes are associated with epidermodysplasia verruciformis. *Nat Genet*. 2002;32(4):579–581.
95. de Jong SJ, et al. The human CIB1-EVER1-EVER2 complex governs keratinocyte-intrinsic immunity to β-papillomaviruses. *J Exp Med*. 2018;215(9):2289–2310.
96. Kerner G, et al. Inherited human IFN-γ deficiency underlies mycobacterial disease. *J Clin Invest*. 2020;130(6):3158–3171.
97. Reed LJ, Muench H. A simple method of estimating fifty per cent endpoints. *Am J Epidemiol*. 1938;27(3):493–497.
98. Minegishi Y, et al. Human tyrosine kinase 2 deficiency reveals its requisite roles in multiple cytokine signals involved in innate and acquired immunity. *Immunity*. 2006;25(5):745–755.
99. Fuchs S, et al. Tyrosine kinase 2 is not limiting human antiviral type III interferon responses. *Eur J Immunol*. 2016;46(11):2639–2649.
100. Sarrafzadeh SA, et al. A new patient with

inherited TYK2 deficiency. *J Clin Immunol*. 2020;40(1):232–235.
101. Boisson-Dupuis S, et al. Tuberculosis and impaired IL-23-dependent IFN-γ immunity in humans homozygous for a common *TYK2* missense variant. *Sci Immunol*. 2018;3(30):eaau8714.
102. Nemoto M, et al. Compound heterozygous TYK2 mutations underlie primary immunodeficiency with T-cell lymphopenia. *Sci Rep*. 2018;8(1):6956.
103. Eletto D, et al. Biallelic JAK1 mutations in immunodeficient patient with mycobacterial infection. *Nat Commun*. 2016;7:13992.
104. Burns C, et al. A novel presentation of homozygous loss-of-function STAT-1 mutation in an infant with hyperinflammation — a case report and review of the literature. *J Allergy Clin Immunol Pract*. 2016;4(4):777–779.
105. Chapgier A, et al. A partial form of recessive STAT1 deficiency in humans. *J Clin Invest*. 2009;119(6):1502–1514.
106. Kong XF, et al. A novel form of human STAT1 deficiency impairing early but not late responses to interferons. *Blood*. 2010;116(26):5895–5906.
107. Shahni R, et al. Signal transducer and activator of transcription 2 deficiency is a novel disorder of mitochondrial fission. *Brain*. 2015;138(pt 10):2834–2846.
108. Hernandez N, et al. Life-threatening influenza pneumonitis in a child with inherited IRF9 deficiency. *J Exp Med*. 2018;215(10):2567–2585.